Simulation and Prediction of Category 4 and 5 Hurricanes in the High-Resolution GFDL HiFLOR Coupled Climate Model

H. Murakami[1,2], G. A. Vecchi[1,2], S. Underwood[3], T. Delworth[1,2],
A.T. Wittenberg[1], W. Anderson[1], J. -H. Chen[1],
R. Gudgel[1], L. Harris[1], S. -J. Lin[1], and F. Zeng[1]

[1]National Oceanic and Atmospheric Administration/Geophysical Fluid Dynamics Laboratory, Princeton, NJ, USA

[2]Atmospheric and Oceanic Sciences Program, Princeton University, Princeton, NJ, USA

[3]Engility, NOAA/GFDL, Princeton, NJ, USA

Submitted to *the Journal of Climate* on 20 March 2015

Corresponding author address: Hiroyuki Murakami, NOAA/GFDL, 201 Forrestal Rd., Princeton, NJ 08540-6649
E-mail: hir.murakami@gmail.com
Tel: 609-452-5824

Abstract

A new high-resolution Geophysical Fluid Dynamics Laboratory (GFDL) coupled model (HiFLOR) has been developed and used to investigate potential skill in simulation and prediction of tropical cyclone (TC) activity. HiFLOR comprises of high-resolution (~25-km mesh) atmosphere and land components and a more moderate-resolution (~100-km mesh) sea ice and ocean components. HiFLOR was developed from the Forecast Oriented Low Resolution Ocean model (FLOR) by decreasing the horizontal grid spacing of the atmospheric component from 50-km to 25-km, while leaving most of the sub-gridscale physical parameterizations unchanged. Compared with FLOR, HiFLOR yields a more realistic simulation of the structure, global distribution, and seasonal and interannual variations of TCs, and a comparable simulation of storm-induced cold wakes and TC-genesis modulation induced by the Madden Julian Oscillation (MJO). Moreover, HiFLOR is able to simulate and predict extremely intense TCs (categories 4 and 5) and their interannual variations, which represents the first time a global coupled model has been able to simulate such extremely intense TCs in a multi-century simulation, sea surface temperature restoring simulations, and retrospective seasonal predictions.

1. Introduction

Recent advances in dynamical modeling and computational resources have enabled climate simulation, prediction, and projection using high-resolution atmospheric general circulation models (AGCMs: e.g., Walsh et al. 2015). A number of numerical modeling studies have reported that increasing resolution in an atmospheric model leads to improved simulation of intense tropical cyclones (TCs). For example, Oouchi et al. (2006) and Murakami et al. (2012) demonstrated a realistic global distribution of intense TCs in multi-decadal simulations using a 20-km-mesh Meteorological Research Institute (MRI) AGCM. Zhao et al. (2009) also showed a realistic simulation of TCs in multi-decadal simulations using a 50-km mesh Geophysical Fluid Dynamics Laboratory (GFDL) High-Resolution Atmospheric Model (HiRAM). Zhao et al. (2010) showed skill in retrospective seasonal predictions of TC frequency in a number of basins using the 50-km version of HiRAM. Chen and Lin (2011, 2013) conducted retrospective seasonal forecasts for hurricanes using a 25-km mesh HiRAM, revealing a remarkable correlation of 0.96 between observed and the simulated TC counts over the 1991–2010 period. Manganello et al. (2012) reported realistic simulations of global TC frequency and intensity with the European Center for Medium-Range Weather Forecasts (ECMWF) Integrated Forecast System (IFS) at 10-km horizontal resolution. Rathmann et al. (2013) reported that a 25-km-mesh EC-earth model outperformed lower-resolution models, in terms of global TC distribution and the interannual variation of TC genesis frequency. Yamada (2010) conducted future projections using a 14-km-mesh atmospheric model (NICAM), representing the first time that a nonhydrostatic global atmospheric model had been used for climate projections. While the atmospheric resolution required for reliable future climate projections of TCs has not yet been determined, a number of studies have reported that a 60-km mesh may be suitable for such projections (Murakami and Sugi 2010; Walsh et al. 2013).

On the other hand, AGCMs lack in physical accuracy at the air-sea interface that is known to be crucial for TC intensity and development (Emanuel 2003; Hasegawa et al. 2007; Knutson et al. 2001). Sea surface temperature (SST) generally decreases along TC tracks due to cold-water wakes induced by wind-induced ocean mixing (Lloyd and Vecchi 2011), which serves to weaken TC intensity and suppress subsequent TC genesis (Schade and Emanuel 1999; Bender and Ginis 2000; Knutson et al. 2001). Because this negative feedback is neglected in AGCMs, atmosphere and ocean coupled models (CGCMs) are preferable to be used for sensitivity studies, predictions, and climate projections of TC activity. However, because a high-resolution CGCM is still computationally expensive, most state-of-the-art CGCMs incorporate a 50–200-km mesh atmosphere component, which is unable to simulate the most intense TCs. A relatively smaller number of studies (Gualdi et al. 2008, Bell et al. 2013, Kim et al. 2014) have used CGCMs to explore the sensitivity of tropical cyclone activity to changes in greenhouse gases. Therefore, the Intergovernmental Panel on Climate Change (IPCC) fifth assessment report (IPCC 2013) relied on principally on results from high-resolution AGCMs (regional and global) rather than CGCMs for future projections of changes in TC statistics [see Table 14.SM.4a in IPCC (2013)]. High-resolution CGCMs have been shown to be potentially useful tools for the subseasonal to seasonal prediction of hurricane activity (Vitart 2007; Vecchi et al. 2014; Camp et al. 2015; Xiang et al. 2015.a, b); though these results have focused principally on tropical cyclone or hurricane frequency, rather than intense tropical cyclones. Dynamical (e.g., Knutson et al. 2015) or statistical (e.g., Zhao and Held 2010; Villarini and Vecchi 2013) refinements are potential mechanisms to extract intensity information from GCMs that do not explicitly simulate the most intense hurricanes. We here focus, however, on a global CGCM that is able to explicitly simulate intense tropical cyclones.

In this study, we develop a high-resolution CGCM (HiFLOR), with an atmospheric horizontal grid spacing of ~25 km and oceanic horizontal grid spacing of ~100 km. This high-resolution CGCM is developed from a more modest (~50 km) high-resolution CGCM (FLOR) (Vecchi et al. 2014) by reducing the horizontal grid spacing of the atmosphere and land components to ~25 km. The main objective of this study is to elucidate how much influence the horizontal resolution of the atmospheric component exerts on the simulation and seasonal prediction of TCs, with a particular focus on the most intense (Category 4–5) TCs.

The remainder of this paper is organized as follows. Section 2 describes the models, experimental design, and data used in this study. Section 3 assesses the performance of simulations and predictions by the high-resolution CGCM compared with the moderate-resolution CGCM. Finally, Section 4 provides a summary of the results.

2. Methods

a. Models and simulation settings

The models used in this study comprise the GFDL Forecast-oriented Low Ocean Resolution model (FLOR; Vecchi et al. 2014; Jia et al. 2015) and a high atmospheric-resolution version of FLOR (HiFLOR). FLOR is comprises 50-km mesh atmosphere and land components, and 100-km mesh sea ice and ocean components. The atmosphere and land components of FLOR are taken from the Coupled Model version 2.5 (CM2.5; Delworth et al. 2012) developed at GFDL, whereas the ocean and sea ice components are based on the GFDL

Coupled Model version 2.1 (CM2.1; Delworth et al. 2006; Wittenberg et al. 2006; Gnanadesikan et al. 2006). CM2.5 substantially improves near-surface and atmospheric climate simulation relative to CM2.1 (Delworth et al.2012; Doi et al. 2012; Delworth and Zeng 2012) as well as tropical cyclones (Kim et al. 2014). The details of FLOR and its simulation performance are documented in Vecchi et al. (2014), Jia et al. (2015), and Krishnamurthy et al. (2015a). FLOR has been used to understand the change, variability and predictability of global and regional climate, and extremes (Vecchi et al. 2014; Msadek et al. 2014; Winton et al. 2014; Jia et al. 2015; Yang et al. 2015; Krishnamurthy et al. 2015.a,b; Delworth et al. 2015; Zhang and Delworth 2015); real-time seasonal predictions with FLOR are made every month through the North American Multi-Model Experiment for seasonal prediction (NMME; Kirtman et al. 2014).

HiFLOR was developed from FLOR by reducing the horizontal grid spacing of the cubed sphere (Putnam and Lin 2007) atmosphere and land components to a 25-km mesh (Chen and Lin 2011, 2013); physical processes and ocean component were inherited from FLOR with only minor changes to the dynamical core and physical parameterizations. In increasing the dynamical core atmospheric resolution, we halved the dynamical time-step of the model, but kept the “physics” time-step (time-step of the convection, cloud an radiation schemes in the model) the same as FLOR. Among the adjustments, HiFLOR applies a reduction in ocean roughness under the intense wind speeds such as TCs (Moon et al. 2004), as implemented in Chen and Lin (2013), which is primarily relevant to the simulation of intense TC that are not present in the FLOR model. However, we have performed a preliminary investigation of dependency of this parameterization on TC intensity, revealing that the effect is small.

We generate 300-year control climate simulations using both FLOR and HiFLOR by prescribing radiative forcing and land-use conditions representative of the year 1990. The control simulations are so-called “free runs” in which flux adjustments (Magnusson et al. 2013; Vecchi et al. 2014) are not applied. Therefor the FLOR and HiFLOR simulations have biases in their sea surface temperature (SST) climatology; as noted in Vecchi et al. (2014), these SST biases can be a large contributor to biases in the TC climatology and interannual variability. Note that because the control runs are free runs, simulated interannual climate (and TC) variations will not be in phase with those in observations.

We also conducted additional experiments in which simulated sea surface salinity (SSS) and SST are restored to the observational estimates over 1971–2012. The simulated SSS was restored to the monthly climatology from the World Ocean Atlas 2005 (Antonov et al. 2006), while SST was restored to the interannually-varying monthly mean value derived from the UK Met Office Hadley Centre SST product (HadISST1.1; Rayner et al. 2003). To test sensitivity of restoring timescale, the restoring experiments are performed with either a 5-day or a 10-day restoring time scale with three different initial conditions, thereby yielding 6 ensemble simulations each for FLOR and HiFLOR. The restoring experiments, by bringing model SST into closer alignment with that observed, should have their climate variations phased with those observed.

To provide a preliminary assessment of the predictability of intense TCs in HiFLOR, we conducted a pair of 36-member ensemble retrospective seasonal forecasts initialized on July 1st 1997 and 1998. Following Vecchi et al. (2014), 10-month duration predictions are performed after initializing the climate model to observationally constrained conditions. The 36-member initial conditions for ocean and sea ice components were taken from a twelve-member coupled ensemble Kalman filter (EnKF) data assimilation system with CM2.1. Meanwhile, initial conditions for atmosphere and land components were taken from three arbitrary years in the 1990 control simulations with HiFLOR. Therefore, the predictability in these experiments comes entirely from the ocean and sea ice, and may be thought of as a lower bound on the potential prediction skill of a model, because predictability could also arise from atmospheric (particularly stratospheric) and land initialization. Combining the twelve ocean/sea ice initial conditions with the three land/atmosphere intial conditions yields 36 ensemble members.

b. Observational datasets

The observed TC "best-track" data were obtained from the International Best Track Archive for Climate Stewardship (IBTrACS; Knapp et al. 2010) and used to evaluate the TC simulations in the control and restoring experiments, and seasonal predictions. The dataset, which consists of best-track data compiled by the National Hurricane Center (NHC) and the Joint Typhoon Warning Center (JTWC), contains historical TC information regarding the locations of the centers of cyclones, cyclone intensities (maximum 1-minute surface wind speeds), and sea level pressures at 6-hourly intervals. We only used TCs with tropical storm strength or stronger (i.e., TCs possessing 1-min sustained surface winds of 35 kt or greater) during the period 1965–2013. To compare simulated cold wakes induced by TCs with observations (Section 3.b), we used the high resolution SST analysis product of National Oceanic and Atmospheric Administration (NOAA) Optimal Interpolation (OI) 1/4 Degree Daily Sea Surface Temperature Analysis (OISST Version 2; Reynolds et al. 2007) for the period 1982–2012. For evaluation of simulated intraseasonal variations (Section 3.d), we used daily Outgoing Longwave Radiation (OLR) data from the Advanced Very High Resolution Radiometer (AVHRR) (Liebmann and Smith 1996) and upper- (200 hPa) and lower- (850 hPa) tropospheric zonal winds from the National Centers for Environmental Prediction/ National Center for Atmospheric Research (NCEP/NCAR) reanalysis (Kalnay et al. 1996) for the period 1979–2005. To evaluate simulated mean SSTs, HadISST1.1 is used during the period 1979–2013. For the evaluation of simulated mean precipitation, the Climate Prediction Center Merged Analysis of Precipitation (CMAP; Xie and Arkin 1997) is used for the period 1979–2013.

c. Detection algorithm for tropical cyclones

Model-generated TCs were detected directly from 6-hourly output using the following tracking scheme in which sea level pressure (SLP) and the temperature anomaly (t_a) averaged between 300 and 500 hPa are mainly used.

(1) Local minima in a smoothed SLP field are detected. The location of the center is fine-tuned by fitting a biquadratic to the SLP field and placing the center at its minimum.

(2) Closed contours of some specified interval dp (here 2 hPa) are found about each center. The N^{th} contour is identified as the contiguous region surrounding a low of central pressure P, with pressures less than $dp \times N + P$, as found by a “flood fill” algorithm. Hence, the contours need not be circular; however, there is a maximum distance of 3,000 km that the algorithm will search away from the candidate low center.

(3) If the above closed contours are found, the low is counted as a storm center at that time. The tracker then tries to find as many closed contours about that low that it can find without going too far from the low center or running into contours claimed by another low.

The maximum 10-m wind inside the set of closed contours is considered to be the maximum wind speed for the storm at that time.

(4) Warm cores are found through a process similar to the above: closed 2K contours for HiFLOR (1K for FLOR) are sought out about the maximum t_a within a storm's identified contours, not more than 1° apart from the low center. This contour must have a radius less than 3° in distance. If no such core is found, the center is not rejected, but is simply marked as not being a warm-core low.

(5) Storm centers are connected into a track by taking a low center at time $T - dt$, extrapolating its motion forward dt, and then looking for storms within 750 km. Deeper lows get first choice of track.

(6) Final TCs are selected by considering satisfactions of duration conditions as follows.

a. At least 72 hours of total detection lifetime.

b. At least 48 cumulative (not necessarily consecutive) hours of having a warm core.

c. At least 36 consecutive hours of a warm core plus winds greater than 17.5 m s^{-1}.

d. The start (last) time of 24 consecutive hours of a warm core plus winds is assigned to genesis (cyclolysis) time. Location of TC genesis should be equatorward of 40°N.

As a sensitivity test, we also applied different tracking schemes from Zhao et al. (2009) and Murakami et al. (2012), and found similar results.

TC positions are counted for each 2.5° × 2.5° grid box within the global domain at 6-hour intervals. The total count for each grid box is defined as the frequency of occurrence of TCs (TCF). The frequency fields are smoothed using a 9-point moving average weighted by distance from the center of the grid box.

The analyses considered total global (GL) results, and results for seven ocean basins: North Indian Ocean (NIO); western North Pacific (WNP); eastern North Pacific (ENP); North Atlantic (NAT); South Indian Ocean (SIO); and South Pacific Ocean (SPO) (see Fig. 2 for regional boundaries).

3. Results

a. Tropical cyclone distributions

Figure 1a, b compares simulated biases (relative to HadISST1.1) of climatological mean SST for 300-yr simulations of FLOR and HiFLOR. Simulated biases of FLOR are also documented in Vecchi et al. (2014). Overall, the spatial patterns of SST biases in HiFLOR are similar to those in FLOR: both models show substantial cold biases in the NAT and WNP, although HiFLOR shows slightly larger cold biases in the tropics and SIO. However, HiFLOR improves warm bias in ENP and eastern tropical Atlantic. The models also share similar bias patterns in the mean precipitation field (Fig. 1c, d), although the amplitude of the biases is slightly reduced in HiFLOR relative to FLOR, especially in the central Pacific. However, HiFLOR appears to have an increase wet bias over the equatorial Atlantic. Overall, the large-scale climate in HiFLOR and FLOR are relatively comparable. Fig.1

Figure 2 compares observed and simulated distributions of TC tracks during all seasons. The annual mean TC number for each basin is also shown in Fig. 2. Compared with observations (Fig. 2c), HiFLOR (Fig. 2b) reproduces extremely intense TCs of categories 4 and 5 (C4 and C5, respectively) more realistically than FLOR (Fig. 2a). For example, HiFLOR simulates concentrated C5 storms in the Philippine Sea as seen in observations. Although FLOR also captures the concentrated location of intense TCs, FLOR critically underestimates Fig.2

TC intensity due to low horizontal resolution: simulated maximum TC intensity around the Philippine Sea is at most category 2. The simulated annual mean TC number in HiFLOR is improved in the NAT (SIO) in which FLOR critically underestimates (overestimates) TC number. However, the simulated TC numbers in WNP and ENP by FLOR are much closer to observations than HiFLOR.

Figure 3a, b compares the spatial distributions of model biases in TCF for the control simulations. Both models generally show similarities in their biases: overestimates in the WNP, central Pacific, and SIO, and underestimates in the eastern ENP and NAT. Note that HiFLOR shows a larger positive bias in WNP than FLOR, as indicated by the overestimation of TC genesis number (Fig. 2). However, HiFLOR reduces the biases in NIO, SIO, SPO, central Pacific, and NAT, leading to improved simulation of the global distribution of TCs by HiFLOR. This result indicates that the high-resolution model is desirable for accurate simulations of the TC spatial distributions, which is also consistent with previous studies (Murakami and Sugi 2010; Manganello et al. 2012; Walsh et al. 2013; and Murakami et al. 2014a). Fig.3

b. Tropical cyclone intensity and composite structure

As indicated in Section 3a, HiFLOR can simulate intense TCs of C4 and C5. Figure 4 shows more detailed comparisons of TC intensity between FLOR and HiFLOR, revealing that HiFLOR improves lifetime maximum intensity (Fig. 4a) significantly relative to FLOR. Although HiFLOR still underestimates C5 TCs (i.e., >69 m s^{-1}) compared with observations, the probability distribution in HiFLOR is closer to observations than in FLOR. The simulated relationship between maximum wind speed (MWS) and minimum SLP (MSLP) using all the Fig.4

6-hr TC data is also investigated in Fig. 4b. Also shown in the figure is Atkinson and Holiday's (1977) nonlinear regression curve derived from observations in the WNP (dashed black curve). HiFLOR can simulate more intense TCs than FLOR while keeping the observed MWS-MSLP relationship, indicating that the simulated TC structure by HiFLOR is reasonable.

Figure 5a–c compares composite TC structure between FLOR and HiFLOR simulated through the 300-yr control simulations. Composite structures are made for the TCs at their lifetime maximum intensity in the Northern Hemisphere. HiFLOR simulates more intense SLP minima, and more intense wind speeds and precipitation than in FLOR. Both models show that the maximum tangential wind speed is located less than 100 km from the storm center (Fig. 5c), which is consistent with observations (Frank 1984; Murakami et al. 2008). Fig.5

Figure 5d–f compares composite structures of SST cooling in the wake of TCs. Following Lloyd and Vecchi (2011), we used daily mean SST anomaly relative to monthly climatology. SST anomalies at 2 days after storm passages relative to the average over 2 to 12 days before the storm passages were used for the input data. As discussed in Lloyd and Vecchi (2011), surface cooling depends on translation speed and latitude. Thus, we consider nondimensional parameter of V/f where V is translation speed [m s^{-1}] and f is the Coriolis parameter [s^{-1}]. V/f is normalized with 100 km (i.e., 1 unit is 100 km). V/f=1 divides all storms equally. Lloyd and Vecchi (2011) found that surface cooling is larger in V/f <1 (i.e., slow-moving or high-latitude) storms than in V/f >1 (i.e., fast-moving or low-latitude) storms. Thus, composites are made for all storms (>34 kt) with V/f < 1 in this study.

Both FLOR (Fig. 5d) and HiFLOR (Fig. 5e) recover the structure of the observed cold SST wake (Fig. 5f). The cold wake is similar between HiFLOR and FLOR, despite the stronger wind speeds in HiFLOR (e.g., Fig. 4). This may be because most of the samples used for the composites are from relatively weaker phases of the storm lifetime. When composites are made for each TC intensity category, both FLOR and HiFLOR simulate larger surface cooling as TC intensity increases (figure not shown). Lloyd and Vecchi (2011) reported that the observed cold-wake is nonmonotonic: stronger cyclones produces more cooling up to C2 but less or approximately equal cooling for C3–5 TCs. Although Lloyd et al. (2011) reported that this nonmonotonicity is well reproduced by GFDL Hurricane Forecast Model (GHM; Kurihara et al., 1998; Bender et al., 2007), HiFLOR could not reproduce this nonmonotonicity (i.e., the HiFLOR cold-wake is stronger in C3–5 TCs than in C2 TCs). The reason for this discrepancy is under investigation.

Figure 6 shows the composite mean SST anomaly for each day before and after storm passage, indicating that simulated cold wake is generally restored to a steady condition 30 days after storm passage, which is consistent with observations (black line). Figure 6 also indicates that the observed SST does not return to the pre-cyclone condition: SST anomaly remains –0.2K at 30 days after storm passage, which is consistent with the previous study (Lloyd and Vecchi 2011). This irreversible surface cooling is also well simulated by both models. Fig.6

c. Seasonal variations

Figure 7 compares seasonal variation of TC genesis frequency between FLOR and HiFLOR. Although simulated biases in both models are similar to those for CM2.5 as shown in Kim et al. (2014), HiFLOR simulates a more reasonable seasonal cycle of TC genesis frequency. For example, the peak month of TC genesis frequency is improved in the WNP and ENP compared with FLOR. Over the NIO (Fig. 7a), FLOR underestimates (overestimates) TC Fig.7

in pre-monsoon (post-monsoon) season, whereas HiFLOR improves these biases. Although simulated annual mean TC number in WNP appears to be better in FLOR than in HiFLOR (Fig. 2), FLOR underestimates TC number during July–September, whereas HiFLOR simulates reasonable frequency in August and September. Simulated seasonal variations of TC genesis frequency in the Southern Hemisphere are mostly identical between the models. The above improvements in HiFLOR relative to FLOR (or CM2.5) are consistent with the previous work of Murakami and Sugi (2010), who noted that increasing horizontal resolution leads to improved seasonal variation of TC frequency for most ocean basins.

d. Interannual variation

The El Niño-Southern Oscillation (ENSO) is one of the primary drivers of interannual variations in TC activity (Lander 1994; Chen et al. 1998; Wang and Chan 2002; Wu et al. 2004; Camargo and Sobel 2005), and a fundamental source of interannual TC predictability (Vecchi et al. 2014). Figure 8 compares simulated composite anomalies of TCF for each warm (El Niño) and cold (La Niña) phase of ENSO during August–October (ASO). Here, we computed SST averaged over the Niño-3 region (5°S–5°N, 90°W –150°W) and Niño-4 region (5°S–5°N, 160°E–150°W) for each year, and the anomaly is computed by subtracting the climatological mean value. El Niño (La Niña) years correspond to years in which the Niño-3 or Niño-4 SST anomalies exceed one (minus one) standard deviation.

Fig.8

The observations (Fig. 8a, e) reveal marked southeast-northwest contrast in TCF in the WNP as reported in Wang and Chan (2002). Overall, both FLOR (Fig. 8b, f) and HiFLOR (Fig. 8c, g) faithfully reproduce the contrasting features. However, during El Niño (La Niña) years, the simulated peak of positive (negative) anomalies in FLOR extends further east of the dateline in the Pacific relative to observations. Simulated location of peak in positive anomaly in WNP during El Niño years is also closer to observations in HiFLOR (Fig. 8c) than in FLOR (Fig. 8b). In addition, during El Niño years, the inhabitation of TCF in ENP is more pronounced in FLOR than HiFLOR. The above discrepancies between FLOR and observations are documented in Vecchi et al. (2014) and Krishnamurthy et al. (2015b). They attribute those inconsistencies to a stronger ENSO in FLOR than observed. Indeed, the simulated standard deviation of the Niño-3.4 index is 1.5K, 1.0K and 0.8K in FLOR, HiFLOR, and observations, respectively, revealing that the biases in ENSO amplitude are reduced in HiFLOR.

During La Niña years, both models show positive anomalies in the ENP (Fig. 8f, g), whereas observations show negative anomalies (Fig. 8e). Krishnamurthy et al. (2015b) reported that in FLOR, La Niña reduces the number of days with strong vertical wind shear and the location of the reduction is co-located with the main TC genesis region in ENP, leading to opposite relation between La Niña and TCF anomaly in FLOR compared to observations. Although sign of anomaly is different from observations, the bias of positive anomaly in ENP during La Niña years is reduced in HiFLOR.

Because the control simulations by FLOR and HiFLOR are free CGCM runs, their simulated year-by-year TC variations are independent of the variations in observations. Here, we conducted additional SSS and SST restoring ensemble experiments, in which the simulated SST is restored to interannually-varing observations at 5-day timescale with three different initial conditions. To test sensitivity of restoring timescale and increase ensemble size, a parallel set of experiments with 10-day restoring time-scale is also applied, thereby yielding 6 ensemble members in total for each model (see Methods section). The difference in TC simulation between 5-day and 10-day restoring time scales was small for both FLOR and HiFLOR (figure not shown), so we treat all six members as a single population from each model. Figure 9a compares interannual variation of TC genesis number in the NAT between FLOR (blue) and HiFLOR (red). HiFLOR simulates the observed interannual variations, as well as the long-term linear trend better than FLOR. These results are consistent with previous studies of Murakami and Sugi (2010), Manganello et al. (2012), Strachan et al. (2013), and Rathmann et al. (2013), who noted that increasing horizontal resolution yields higher skills in simulating observed interannual variation of TC frequency.

Fig.9

Table 1 summarizes rank correlations between simulations and observations. Overall, HiFLOR outperforms FLOR for both all storms (Table 1a) and hurricanes (Table 1b) except for NIO and WNP. Significant improvements can be seen in the variation of hurricanes (Fig. 9b): HiFLOR reproduces the observed interannual variation and trend of hurricane count, whereas FLOR does not reproduce them as skilfully. HiFLOR yields higher correlations for hurricanes than those for all TCs in the ENP, NAT, and SIO (Table 1a, b). A number of previous studies have shown similarly high correlations with observed TC numbers in the NAT, using similar experimental settings (e.g., LaRow et al. 2008; Zhao et al. 2009; Murakami and Wang et al. 2010; Strachan et al. 2013). Specifically, Knutson et al. (2008) showed a high correlation of simulated and observed hurricane counts in the NAT, using a regional model with restoring of both the SST and large-scale fields toward observations. However, the present study with HiFLOR is the first to show such high correlations for C4 and C5 hurricanes with a global coupled model (Fig. 9c and Table 1c). These results highlight potential predictability of extremely intense TCs if the SSTs can be predicted accurately.

Tab.1

Because the SST biases are much smaller in the restoring experiments, these experiments allow us to assess the extent to which simulated biases in the control CGCM simulations arise from biases in SST as opposed to the biases in the atmosphere component. Figure 3c shows model biases in TCF in the restoring experiments in HiFLOR. Compared to those in the control simulation (Fig. 3b), the restoring experiments reduce the biases in the central Pacific, SPO, and NAT, indicating that these biases in climatological TC simulation in the control simulation have a substantial element due to the SST biases. On the other hand, the overestimation of TCF in the Indian Ocean remains and that in WNP becomes larger, indicating these biases may be intrinsic to the atmospheric component.

Figure 8d, h shows composite anomalies of TCF for each phase of ENSO simulated by the restoring experiments using HiFLOR. Compared to the control simulation (Fig. 8c, g), the restoring experiments substantially improve the spatial patterns. The restoring experiments simulate clear peaks of anomalies in WNP, which are closer to observations than for the control experiment. Moreover, the restoring experiments reproduce the observed negative anomaly during La Niña years in ENP (Fig. 8h), whereas the control simulation fails to simulate the negative anomaly (Fig. 8g). Vecchi et al. (2014) and Krishnamurthy et al. (2015b) reported similar improvements using the flux-adjusted version of FLOR, in which model's momentum, enthalpy and freshwater fluxes from atmosphere to ocean are adjusted to bring the model's long-term climatology of SST and surface wind stress closer to observations. They concluded that this bias could be corrected by simulating the correct location of reduction in vertical wind shear in ENP during La Niña years, which is related to the strength of ENSO.

Figure S1 in the supplemental material also compares simulated TC intensity between the control simulation and the restoring experiments. Although the difference between the control simulation and restore experiments in FLOR (blue lines) is not clear, the restoring experiments in HiFLOR (red line with rectangles) significantly increases TC intensity relative to the control simulation (red line with circles). An additional experiment, for which the simulated SSS and SST are restored to the simulated climatological mean of the HiFLOR control simulation at 5-day timescale (green line with triangles), reveals a similar TC intensity to that of the control simulation. The above results indicate that the more intense TCs in the restoring experiments relative to the control simulation are connected to differences in the mean state rather than to the nudging itself.

e. Intraseasonal variations

Intraseasonal variability in the atmosphere-ocean coupled system plays an important role in modulating TC genesis, and represent a potential source of TC predictability on greater than weekly time-scales (e.g., Xiang et al. 2015a,b). Maloney and Hartmann (2000) reported that hurricanes in the Gulf of Mexico and western Caribbean are strongly modulated by wind anomalies induced by the Madden-Julian oscillation (MJO). TC genesis frequency in the WNP also experiences a significant intraseasonal variation (Yamazaki and Murakami 1989; Hartmann et al. 1992; Liebmann et al. 1994; Fu et al. 2007). In particular, Li and Zhou (2013) showed that in the WNP, northeastward-propagating MJO predominantly controls the basin-wide TC frequency. A number of numerical studies have showed that the MJO provides a source of predictability for TC genesis (Fudeyasu et al. 2008; Fu and Hsu 2011; Vitart, 2009; Belanger et al. 2010; Elsberry et al. 2010; Xiang et al. 2015a). Therefore, it is important to evaluate whether models adequately simulate the MJO and its association with TC genesis.

Figure 10 compares Wheeler-Kiladis diagrams (Wheeler and Kiladis 1999; Kim et al. 2009) which show observed and simulated zonal wavenumber-frequency power spectra of meridionally symmetric and antisymmetric components of OLR, divided by the background power. The simulated MJO signals in the period range of 30–80 days in both FLOR and HiFLOR are strong and comparable to each other, although the simulated signals are slightly weaker than observed. When the two models are compared, HiFLOR simulates stronger atmospheric Kelvin waves and mixed Rossby-gravity waves (MRG), which are closer to observations than for FLOR. Fig.10

Figure 11 represents composites of TC genesis locations superposed on anomalies of OLR and wind vectors at 850 hPa for each MJO phase during boreal summer (May–October). Figure S2 in the supplemental material shows these during boreal winter (November–April). Note that these composites are made when the MJO index exceeds one standard deviation for each phase (i.e., the active MJO phase). Following Wheeler and Hendon (2004), the MJO index is obtained from the magnitude of first two principal components of the multivariate empirical orthogonal functions (EOFs) using daily mean OLR, 850 hPa zonal wind, and 200-hPa zonal wind. Observations indicate that events of TC genesis are more frequent during the MJO active phase for each basin, as reported in Maloney and Hartman (2000) and Li and Zhou (2013). This modulation of TC genesis is also well simulated in the 300-yr control simulations of FLOR and HiFLOR. Figure 12 illustrates the TC genesis rate for each MJO phase in each basin. Overall, the MJO simulations of FLOR and HiFLOR are similar, and both models reproduce the observed enhancement of TC genesis during the active MJO phase. Fig. 11 Fig. 12

Although MJO is reasonably simulated in both HiFLOR and FLOR, both models substantially overestimate (underestimate) TC genesis frequency in WNP (ENP and NAT). On the other hand, Murakami et al. (2012) reported that the 20-km-mesh MRI-AGCM yielded a realistic simulation of the global TC distribution, although Yoshimura et al. (2015) reported that the model's MJO is much weaker than observed. Moreover, Yamada et al. (2010) showed that NICAM substantially underestimated TC genesis frequency in ENP and NAT, while Miura et al. (2007) showed that it simulated a strong MJO. These results, in combination with present study, suggest that model performance in simulating the global TC distribution may be only weakly related to performance in simulating the MJO.

f. Retrospective seasonal forecast for 1997/1998

To provide a preliminary assessment of the predictability of intense TCs in HiFLOR, we conducted a couplet of 36-member ensemble retrospective seasonal forecasts initialized on July 1st in 1997 and 1998. These start dates were chosen as they allow us to target the extreme El Niño and La Niña events of 1997–98 and 1998–99, respectively. The boreal summer in 1997 was in sharp contrast to that in 1998 in terms of global TC activity (Pasch et al. 2001; Du et al. 2011; Tao et al. 2012; Zhao et al. 2014). The 1997 TC season is characterized by more frequent and intense TCs in WNP as well as less frequent and weaker TCs in NAT associated with strong El Niño (Fig. 13a). Meanwhile, the 1998 TC anomalies largely oppose to those of 1997, arising from the strong La Niña (Fig. 13b). Of particular interest in this study is to elucidate whether HiFLOR can predict above contrasts in the intense TCs of hurricanes and C45 hurricanes. The contrast in large-scale climate and TCs between these two years provides a useful benchmark for predictability, but the results reported here should not be interpreted as applying broadly to predictive skill for all years.

Fig. 13

Figure 13 shows predicted TC tracks in HiFLOR compared to observations. Note that all TC tracks predicted in the 36-ensemble members are superposed in the figure. Figure 14 Fig. 14 shows the differences in the mean TCF between 1997 and 1998 for each TC intensity category. Figure 15 shows box plots for predicted TC numbers for each TC intensity category Fig. 15 superposed on the observed TC numbers (triangles). The predicted TC tracks in 1998 are concentrated in the South China Sea (Fig. 13d, 14b), whereas those in 1997 expand further east of the open ocean in WNP (Fig. 13c, 14b), which are consistent with observations (Fig. 13b, 14a). Moreover, the observed east-west contrasts in hurricanes and C45 hurricanes in WNP are well predicted in HiFLOR (Fig. 14c–f). The observed contrast in the number of intense TCs in WNP is also predicted in HiFLOR (Fig. 15d, g), although the HiFLOR test forecasts systematically overestimate these numbers relative to observations – much like the other HiFLOR experiments did (Figs. 3, 7). In NAT, predicted mean TC number for all storms in 1998 is two-times larger than that in 1997, which is consistent with observations (Fig. 15c). Moreover, HiFLOR was able to retrospectively predict the observed two-year contrasts in the numbers of hurricanes (Fig. 15f) and C45 hurricanes (Fig. 15i). As for ENP, the observed two-year contrasts in the numbers of all storms and hurricanes are also predicted in HiFLOR (Fig. 15b,e), although HiFLOR underestimates C45 hurricanes (Fig. 15h). Generally, the observed contrasts between 1997 and 1998 in the intense TCs are well retrospectively predicted in HiFLOR, in both relative basin-wide frequency and in the spatial structure of TCF differences between the two years.

4. Summary

We have developed HiFLOR, a high-resolution version of the GFDL Forecaset-oriented Low Ocean Resolution model (FLOR). HiFLOR was developed from FLOR by reducing the horizontal grid spacing of the atmosphere and land components from 50-km to 25-km mesh with only minor changes to the dynamical core physical parameterizations. Two sets of simulations were conducted using HiFLOR: a 300-yr control climate simulation with prescribed radiative forcing and land-use conditions representative of 1990; and restoring experiments over 1971–2012 in which the simulated SSS and SST are restored to the observations at 5-day or 10-day time scales. Simulated TCs are compared with those from similar experiments conducted using FLOR. In addition, a couple of ensemble seasonal predictions for 1997 and 1998 were performed with HiFLOR.

In its control simulation, HiFLOR reproduces the climatological spatial distribution of the global TCs more realistically than FLOR does. In particular, HiFLOR reduces biases in the frequency of TC occurrence in the central Pacific, South Pacific, North Atlantic, and Indian Ocean. The simulated distribution of TC intensity by HiFLOR is also comparable to observations, whereas FLOR cannot simulate intense TCs. HiFLOR is able to simulate extremely intense TCs (Categories 4 and 5) reasonably well compared to observations. The simulated TC intensity in HiFLOR is of comparable skill to that in a high-resolution AGCM reported in Murakami et al. (2012) and Manganello et al. (2012), and to that with double dynamical downscaling reported in Bender et al. (2010) and Knutson et al. (2008, 2013, 2015). However, this study represents the first global coupled climate model to successfully simulate such intense TCs in a multi-century simulation. HiFLOR simulates reasonable structure for the TCs, while also capturing the observed relationship between the maximum surface wind speed and the minimum sea level pressure. The composite TC structure in HiFLOR was compared with FLOR and observations, and revealed that HiFLOR reasonably simulated the location of maximum wind speed and the surface oceanic cold wake induced by the storm's strong wind stresses.

Although HiFLOR appears to inherit model biases from FLOR and CM2.5 in terms of the seasonal cycle of TC frequency, the simulated seasonal cycle has been considerably improved in HiFLOR relative to FLOR. Comparisons between SST-restored versions of FLOR and HiFLOR reveal that HiFLOR more skilfully simulates the interannual variation of TC genesis frequency when compared to FLOR except for NIO and WNP. Specifically, the SST-restored HiFLOR exhibited high correlation coefficients with the observed interannual variations of hurricanes (r=0.77) and categories 4 and 5 hurricanes (r=0.63) in NAT. This is the first time that a global climate model has successfully reproduced the observed year-by-year variations in category 4 and 5 hurricanes under restored-SST experiments. Both FLOR and HiFLOR exhibit a strong 30–80-day Madden-Julian Oscillation, whose active phase enhances TC genesis as observed, indicating potential skill in predicting TC genesis events at intraseasonal time scales. The initial tests for retrospective seasonal forecasts for 1997/1998 TC seasons reveal that HiFLOR has substantial skills in predicting the observed contrasts between 1997 and 1998 in terms of frequency of hurricanes and category 4 and 5 hurricanes and their spatial distributions.

In summary, the use of a higher-resolution atmospheric component appears to be desirable for accurate simulation of TCs. HiFLOR can be also used for attribution studies through idealized experiments to elucidate the contributions of anthropogenic forcing and natural variability to the observed recent upward trend in the frequency of category 4 and 5 hurricanes (Murakami et al. 2014b). Although HiFLOR has a substantially improved TC climatology compared with FLOR, HiFLOR still has a substantial bias in TC frequency in the WNP. Although, as Vecchi et al. (2014) reported, simulations of the TC climatology and temporal variations can be substantially improved by correcting ocean biases via artificial flux adjustments, it will ultimately be desirable to minimize these biases through continued improvements in model formulation.

Acknowledgments The authors thank Dr. Baoqiang Xiang and Dr. Wei Zhang for their suggestions and comments.

References

Antonov, J. I., R. A. Locarnini, T. P. Boyer, A. V. Mishonov, and H. E. Garcia, 2006: *Salinity*. Vol. 2, *World Ocean Atlas 2005,* NOAA Atlas NESDIS 62, 182 pp.

Atkinson, G. D., and C. R. Holiday, 1977: Tropical cyclone minimum sea level pressure/maximum sustained wind relationship for the western North Pacific. *Mon. Wea. Rev.*, **105**, 421–427.

Belenger, J. I., J. A. Curry, and P. J. Webster, 2010: Predictability of North Atlantic tropical cyclone activity on intraseasonal time scales. *Mon. Wea. Rev.*, **138,** 4362–4374.

Bell, R., J. Strachan, P.L. Vidale, K. Hodges, M. Roberts, 2013: Response of tropical cyclones to idealized climate change experiments in a global high-resolution coupled general circulation model. *J. Climate,* **20,** 7966–7980.

Bender, M. A., and I. Ginis, 2000: Real-case simulations of hurricane-ocean interaction using a high-resolution coupled model: Effects on hurricane intensity. *Mon. Wea. Rev.*, **128,** 917–946.

Bender, M. A., I. Ginis, R. E. Tuleya, B. Thomas, and T. Marchok, 2007: Real-case simulations of hurricane-ocean interaction using a high-resolution coupled model: Effects on hurricane intensity. *Mon. Wea. Rev.*, **128,** 917–946.

Bender, M. A., T. R. Knutson, R. E. Tuleya, J. J. Sirutis, G. A. Vecchi, S. T. Garner, and I. M. Held, 2010: Modeled impact of anthropogenic warming on the frequency of intense Atlantic hurricanes. *Science,* 327, 454–458.

Camargo, S. J. and A.H. Sobel, 2005: Western North Pacific tropical cyclone intensity and ENSO. *J. Climate,* **18,** 2996–3006.

Camp, J., M. Roberts, C. MacLachlan, E. Wallace, L. Hermanson, A. Brookshaw, A. Arribas, and A.A. Scaife, 2015: Seasonal forecasting of tropical storms using the Met Office GloSea5 seasonal forecast system. Quart. J. Roy. Meteor. Soc., doi:10.1002/qj.2516.

Chen, J.-H. and S.-J. Lin, 2011: The remarkable predictability of inter-annual variability of Atlantic hurricanes during the past decade. *Geophys. Res. Lett.,* **38,** L11804.

Chen, J.-H. and S.-J. Lin, 2013: Seasonal predictions of tropical cyclones using a 25-km-resolution general circulation model. *J. Climate,* **26,** 380–398.

Chen, T.-C., S. P. Weng, N. Yamazaki, and S. Kiehne, 1998: Interannual variation in the tropical cyclone formation over the western North Pacific. *Mon. Wea. Rev.*, **126,** 1080–1090.

Delworth, T. L., and co-authors, 2006: GFDL's CM2 global coupled climate models. Part I: Formulation and simulation characteristics. *J. Climate*, **19,** 643–674.

Delworth, T. L., and co-authors, 2012: Simulated climate and climate change in the GFDL CM2.5 high-resolution coupled climate model. *J. Climate*, **25,** 2755–2781.

Delworth, T. L., and F. Zeng, 2012: Multicentennial variability of the Atlantic meridional overturning circulation and its climatic influence in a 4000 year simulation of the GFDL CM2.1 climate model. *Geophys. Res. Lett.,* **39,** L13702.

Delworth, T. L., F. Zeng, A. Rosati, G. Vecchi, and A. Wittenberg, 2015: A link between the hiatus in global warming and North American drought. *J. Climate*, In press.

Doi, T., G. A. Vecchi, A. J. Rosati, and T. L. Delworth, 2012: Biases in the Atlantic ITCZ in seasonal-interannual variations for a corse- and a high-resolution coupled climate model. *J. Climate*, **25,** 5494–5511.

Du, Y., L. Yang, and S. P. Xie, 2011: Tropical Indian Ocean influence on Northwest Pacific tropical cyclones in summer following strong El Nino. *J. Climate*, **24,** 315–322.

Elsberry, R. L., M. S. Jordan, and F. Vitart, 2010: Predictability of tropical cyclone events on intraseasonal timescales with the ECMWF monthly forecast model. *Asia-Paficic J. Atmos. Sci.,* **46,** 135–153.

Emanuel, K, 2003: Tropical cyclones. *Annu. Rev. Earth Planet. Sci.* **31,** 75–104.

Frank W. M., 1984: A composite analysis of the core of a mature hurricane. *Mon. Wea. Rev*.,**112**, 2401–2420.

Fu, B., T. Li, M. S. Peng, and F. Weng, 2007: Analysis of tropical cyclogenesis in the western North Pacific for 2000 and 2001. *Wea. Forecasting,* **22,** 763–780.

Fu, X., and P.-C. Hsu, 2011: Extended-range ensemble forecasting of trpical cyclogenesis in the northern Indian Ocean: Modulation of Madden-Julian Oscillation. *Geophys. Res. Lett.,* **38,** L15803.

Fudeyasu, H., Y. Wang, M. Satoh, T. Nasuno, H. Miura, and W. Yanase, 2008: The global cloud-system-resolving model NICAM successfully simulated the lifecycloes of two real tropical cyclones. *Geophys. Res. Lett.,* **35,** L22808.

Gnanadesikan, A., and co-authors, 2006: GFDL's CM2 global coupled climate models. Part II: The baseline ocean simulation. *J. Climate*, **19,** 675–697.

Gualdi, S., E. Scoccimarro, and A. Navarra, 2008: Changes in tropical cyclone activity due to global warming: Results from a high-resolution coupled general circulation model. *J. Climate*, **20**, 5204–5228.

Hamed, K. H., and A. R. Rao, 1998: A modified Mann-Kendall trend test for autocorrelated data. *J. Hydrol.*, **204,** 182–196.

Hartmann, D. L., M. L. Michelsen, and S. A. Klein, 1992: Seasonal variations of tropical intraseasonal oscillations: A 20-25-day oscillation in the Western North Pacific. *J. Atmos. Sci.,* **49,** 1277–1289.

Hasegawa A., and S. Emori, 2007: Effect of air-sea coupling in the assessment of CO_2-induced intensification of tropical cyclone activity. *Geophys. Res. Lett.,* **34,** L05701.

IPCC, 2013: Climate Change 2013: The Physical Science Basis. Contribution of Working Group I to the Fifth Assessment Report of the Intergovern-mental Panel on Climate Change [Stocker, T.F., D. Qin, G.-K. Plattner, M. Tignor, S.K. Allen, J. Boschung, A. Nauels, Y. Xia, V. Bex and P.M. Midgley (eds.)]. Cambridge University Press, Cambridge, United Kingdom and New York, NY, USA, 1535 pp.

Jia, L., and co-authors, 2015: Improved seasonal prediction of temperature and precipitation over land in a high-resolution GFDL climate model. *J. Climate*, **28,** 2044–2062.

Kalnay, E., and co-authors, 1996: The NCEP/NCAR 40-Year Reanalysis Project. *Bull. Amer. Meteor. Soc.,* **77,** 437–471.

Kirtman, B. P, and co-authors, 2014: The North American Multimodel Ensemble: Phase-1 seasonal-to-interannual prediction; Phase-2 toward developing intraseasonal prediction. *Bull. Amer. Meteor. Soc.,* **95,** 585–601.

Kim, D., and co-authors, 2009: Application of MJO simulation diagnostics to climate models. *J. Climate*, **22,** 6413–6436.

Kim, H.-S., and co-authors, 2014: Tropical cyclone simulation and response to CO_2 doubling in the GFDL CM2.5 high-resolution Coupled climate model. *J. Climate*, **27,** 8034–8054.

Knapp, K. R., M. C. Kruk, D. H. Levinson, H. J. Diamond, and C. J. Neuman, 2010: The international best track archive for climate stewardship (IBTrACS): Unifying tropical cyclone best track data, *Bull. Amer. Meteor. Soc.*, **91**, 363–376.

Knutson, T. R., R. E. Tuleya, W. Shen, I. Ginis, 2001: Impact of CO_2-induced warming on hurricane intensities as simulated in a hurricane model with ocean coupling. *J. Climate*, **14,** 2458–2468.

Knutson, T. R., J. J. Sirutis, S. T. Garner, G. A. Vecchi, and I. M. Held, 2008: Simulated reduction in Atlantic hurricane frequency under twenty-first-century warming condition. *Nature Geocience,* **1,** 359–364.

Knutson, T. R., and co-authors, 2013: Dynamical downscaling projections of twenty-first-century Atlantic hurricane activity: CMIP3 and CMIP5 model-based scenarios. *J. Climate*, **26,** 6591–6617.

Knutson, T. R., J. J. Sirutis, M. Zhao, R. E. Tuleya, M. Bender, G.A. Vecchi, G. Villarini, and D. Chavas, 2015: Global projections of intense tropical cyclone activity for the late 21st century from dynamical downscaling of CMIP5/RCP4.5 scenarios. *J. Climate*, submitted.

Kurihara, Y., R. E. Tuleya, and M. A. Bender, 1998: The GFDL Hurricane Prediction System and its performance in the 1995 hurricane season. *Mon. Wea. Rev.*, **126,** 1306–1322.

Krishnamurthy, L., G. A. Vecchi, R. Msadek, A. Wittenberg, T. Delworth, and F. Zeng, 2015a: The seasonality of the Great Plains low-level jet and ENSO relationship. *J. Climate*, In press.

Krishnamurthy, L,, and co-authors, 2015b: Effect of extreme ENSO events on regional tropical cyclone activity in high-resolution model. *J. Climate*, submitted.

Lander, M. A., 1994: An exploratory analysis of the relationship between tropical storm formation in the western North Pacific and ENSO. *Mon. Wea. Rev.*, **122,** 636-651.

LaRow, T. E., Y.-K. Lim, D. W. Shin, E. P. Chassignet, and S. Cocke, 2008: Atlantic basin seasonal hurricane simulations. *J. Climate,* **21,** 3191–3206.

Li, R. C. Y., and W. Zhou, 2013: Modulation of western North Pacific tropical cyclone activity by the ISO. Part I: Genesis and intensity. *J. Climate*, **26,** 2904–2918.

Liebmann, B., H. H. Hendon, and J. D. Glick, 1994: The relationship between tropical cyclones of the Western Pacific and Indian Oceans and the Madden-Julian oscillation. *J. Meteor. Soc. Japan*, **72,** 401–412.

Liebmann B., and C. A. Smith, 1996: Description of a complete (interpolated) outgoing longwave radiation dataset. *Bull. Amer. Meteor. Soc.,* **77,** 1275–1277.

Lloyd, I. D., and G. A. Vecchi, 2011: Observational evidence for oceanic controls on hurricane intensity. *J. Climate*, **24,** 1138–1153.

Lloyd, I. D., T. Marchok, and G. A. Vecchi, 2011: Diagnostics comparing sea surface temperature feedbacks from operational hurricane forecasts to observations. *J. Adv. Model. Earth Syst.*, **3,** M11002.

Manganello, and co-authors, 2012: Tropical cyclone climatology in a 10-km global atmospheric GCM: Toward weather-resolving climate modeling. *J. Climate*, **24,** 3867–3893.

Magnusson, L., M. Alonso-Balmaseda, S. Corti, F. Molteni, and T. Stockdale, 2013: Evaluation of forecast strategies for seasonal and decadal forecasts in presence of systematic model errors. *Climate Dyn.* **41,** 2393–2409.

Maloney, E. D., and D. L. Hartmann, 2000: Modulation of hurricane activity in the Gulf of Mexico by the Madden-Julian oscillation. *Science,* **287,** 2002–2004.

Miura, H., M. Satoh, T. Nasuno, A. T. Noda, and K. Oouchi, 2007: A Madden-Julian oscillation event simulated using a global cloud-resolving model, *Science,* **318,** 1763–1765.

Moon, I.-J., I. Ginis, and T. Hara, 2004: Effect of surface waves on air-sea momentum exchange. Part II: Behavior of drag coefficient under tropical cycloens. *J. Atmos. Sci.*, **61,** 2334–2348.

Msadek, R., G.A. Vecchi, M. Winton, R.G. Gudgel, 2014: Importance of initial conditions in sseasonal predictions of Arctic sea ice extent. *Geophys. Res. Lett.,* **41,** 5208–5215.

Murakami, H., T. Matsumura, R. Sakai, A. Noda, and S. Kusunoki, 2008: Verification typhoon forecasts for a 20km-mesh high-resolution global model. *J. Meteor. Soc. Japan*, **86**, 669–698.

Murakami, H., and M. Sugi, 2010: Effect of model resolution on tropical cyclone climate projections. *SOLA*, **6,** 73–76.

Murakami, H., and B. Wang, 2010: Future change of North Atlantic tropical cyclone tracks: Projection by a 20-km-mesh global atmospheric model. *J. Climate*, **23**, 2699–2721.

Murakami, H., and co-authors, 2012: Future changes in tropical cyclone activity projected by the new high-resolution MRI-AGCM. *J. Climate*, **25,** 3237–3260, doi: 10.1175/JCLI-D-11-00415.1.

Murakami, H., B. Wang, T. Li, and A. Kitoh, 2013: Projected increase in tropical cyclones near Hawaii. *Nat. Climate Change*, **3**, 749-754.

Murakami, H., P. –C. Hsu, O. Arakawa, and T. Li, 2014a: Influence of model biases on projected future changes in tropical cyclone frequency of occurrence. *J. Climate*, **27,** 2159–2181.

Murakami, H., T. Li, and P. –C. Hsu, 2014b: Contributing factors to the recent high level of Accumulated Cyclone Energy (ACE) and Power Dissipation Index (PDI) in the North Atlantic. *J. Climate*, **27,** 3023–3034.

Oouchi, K., J. Yoshimura, H. Yoshimura, R. Mizuta, S. Kusunoki, and A. Noda, 2006: Tropical cyclone climatology in a global-warming climate as simulated in a 20km-mesh global atmospheric model: Frequency and wind intensity analysis. *J. Meteor. Soc. Japan*, **84,** 259–276.

Pasch, R. J., L.A. Avila, and J. L. Guiney, 2001: Atlantic Hurricane season of 1998. *Mon. Wea. Rev.*, **129,** 3085–3123.

Putman, W.M., and S.-J. Lin, 2007: Fineite-volume transport on various cubed-sphere grids. *J. Comput. Phys.* 227(1), 55–78.

Rayner, N. A., D. E. Parker, E. B. Horton, C. K. Folland, L. V. Alexander, and D. P. Rowell, 2003: Global analysis of sea surface temperature, sea ice, and night marine air temperature since the late nineteenth century. *J. Geophys. Res*., **108**, 4407.

Rathmann, N. M., S. Yang, and E. Kaas, 2013: Tropical cyclones in enhanced resolution CMIP5 experiments. *Climate Dyn.* **42,** 665–681.

Raynolds, R., T. M. Smith, C. Liu, D. B. Chelton, K. S. Casey, and M. G. Schlax, 2007: Daily high-resolution blended analyses for sea surface temperature. *J. Climate*, **20,** 5473–5496.

Shade, L., and K. Emanuel, 1999: The ocean's effect on the intensity of tropical cyclones: Results from a simple coupled atmosphere-ocean model. *J. Atmos. Sci.*, **56,** 642–651.

Strachan, J., P. L. Vidale, K. Hodges, M. Roberts, and M. –E. Demory, 2013: Investigating global tropical cyclone activity with a hierarchy of AGCMs: The role of model resolution. *J. Climate*, **26,** 133–152.

Tao, L., L. Wu, Y. Wang, and J. Yang, 2012: Influence of tropical indian ocean warming and ENSO on tropical cyclone activity over the Wstern North Pacific. *J. Meteor. Soc. Japan*, **90**, 127–144.

Vecchi, G. A., and co-authors, 2014: On the seasonal forecasting of regional tropical cyclone activity. *J. Climate*, **27,** 7994–8016.

Villarini, G., and G. A. Vecchi, 2013: Projected increases in North Atlantic tropical cyclone intensity from CMIP5 models. *J. Climate*, **26,** 3231–3240.

Vitart, F., and co-authors, 2007: Dynamically-based seasonal forecasts of Atlantic tropical storm activity issued in June by EUROSIP. *Geophys. Res. Lett.,* **34,** L16815.

Vitart, F., 2009: Impact of the Madden Julian Oscillation on tropical cyclones and risk of landfall in the ECMWF forecasting system. *Geophys. Res. Lett.,* **36,** L15802.

Walsh, K., S. Lavender, E. Scoccimarro, and H. Murakami, 2013: Resolution dependence of tropical cyclone formation in CMIP3 and finer resolution models. *Clim. Dyn.* **40,** 585–599.

Walsh, K. J. E., and co-authors, 2015: Hurricanes and climate: The U.S. CLIVAR working group on hurricanes. , *Bull. Amer. Meteor. Soc.*, In press.

Wang, B., and J. C. L. Chan, 2002: How strong ENSO events affect tropical storm activity over the western North Pacific. *J. Climate,* **15,** 1643–1658.

Wheeler, M., and G. N. Kiladis, 1999: Convectively coupled equatorial waves: Analysis of clouds and temperature in the wavenumber-frequency domain. *J. Atmos. Sci.,* **56,** 374–399.

Wheeler, M., and H. H. Hendon, 2004: An all-season real-time multivariate MJO index: Development of an index for monitoring and prediction. *Mon. Wea. Rev.*, **132,** 1917–1932.

Winton, M., W.G. Anderson, T. L. Delworth, S.M. Griffies, W. J. Hurlin, and A. Rosati, 2014: Has coarse ocean resolution biased simulations of transient climate sensitivity? *Geophys. Res. Lett.,* **41,** 8522–8529.

Wittenberg, A. T., A. Rosati, N. –C. Lau, and J. J. Ploshay, 2006: GFDL's CM2 global coupled climate models. Part III: Tropical pacific climate and ENSO. *J. Climate*, **19,** 698–722.

Wu, L., and B. Wang, 2004: Assessing impact of global warming on tropical cyclone tracks. *J. Climate,* **17,** 1686–1698.

Xiang, B., S.-J. Lin, M. Zhao, S. Zhang, G. Vecchi, T. Li, X. Jiang, L. Harris, J.-H. Chen, 2015a: Beyond weather time scale prediction for Hurricane Sandy and super typhoon Haiyan in a global climate model. *Mon. Wea. Rev.*, **143,** 524–535.

Xiang, B., M. Zhao, X. Jiang, S.-J. Lin, T. Li, X. Fu, G. Vecchi, A. Sobel, I.-S. Kang, P.-C. Hsu, E. Maloney, D. Kim, 2015b: 3-4 week MJO prediction skill in a GFDL coupled model. *Mon. Wea. Rev.*, submitted.

Xie, P., and P. A. Arkin, 1997: Global precipitation: A 17-year monthly analysis based on gauge observations, satellite estimates, and numerical model outputs. *Bull. Amer. Meteor. Soc.,* **78,** 2539–2558.

Yang, X., and co-authors, 2015: Seasonal predictability of extratropical storm tracks in GFDL's high-resolution climate prediction model. *J. Climate*, In press.

Yamada, Y., K. Oouchi, M. Satoh, H. Tomita, and W. Yanase, 2010: Projection of changes in tropical cyclone activity and cloud height due to greenhouse warming: Global cloud-system-resolving approach. *Geophys. Res. Lett.,* **37,** L07709.

Yamazaki, N. and M. Murakami, 1989: An intraseasonal amplitude modulation of the short-term tropical disturbances over the Western Pacific. *J. Meteor. Soc. Japan*, **67,** 791–807.

Yoshimura, H, R. Mizuta, and H. Murakami, 2015: A spectral cumulus parameterization scheme interpolating between two convective updrafts with semi-Lagrangian calculation of transport by compensatory subsidence. *Wea. Rev.*, In press.

Zhang, L., and T.L. Delworth, 2015: Analysis of the characteristics and mechanisms of the Pacific Decadal Oscillation in a suite of coupled models from the Geophysical Fluid Dynamics Laboratory. *J. Climate*, submitted.

Zhao, H., P.-S. Chu, P.-C. Hsu, and H. Murakami, 2014: Exploratory analysis of extremely low tropical cyclone activity during the late-season of 2010 and 1998 over the Western North Pacific and South China Sea. *J. Adv. Model. Earth Syst.* **06**.

Zhao, M., I. M. Held, S.-J. Lin, and G. A. Vecchi, 2009: Simulations of global hurricane climatology, interannual variability, and response to global warming using a 50km resolution GCM. *J. Climate*, **22,** 333–363.

Zhao, M., and I.M. Held, 2010: An analysis of the effect of global warming on the intensity of Atlantic hurricanes using a GCM with statistical refinement. *J. Climate*, **23,** 6382–6393.

Zhao, M., I.M. Held, and G.A. Vecchi, 2010: Retrospective forecasts of the hurricane season using a global atmospheric model assuming persistence of SST anomalies. Mon. Wea. Rev., 138, 3858–3868.

List of Tables

Table 1 (a) Rank correlation coefficients between the observed and simulated interannual variability of TC genesis number in the SST restored experiments for each basin. (b, c) As in (a), but for TCs with hurricane maximum winds >64 kt, and intensity categories 4 and 5 (>114 kt), respectively. 6-member SST-restored ensemble experiments are conducted using 5-day and 10-day restoring timescales each for HiFLOR and FLOR. Statistical significance is highlighted according to the level of significance: 99%, 95%, and 90% (see footnotes).

List of Figures

FIG. 1. Simulated biases in climatological mean SST [K] relative to HadISST1.1 during all seasons for (a) FLOR and (b) HiFLOR. (c), (d) As in (a), (b), but for precipitation [mm day^{-1}] relative to CMAP.

FIG. 2. Global distribution of TC tracks during all seasons for 300-year control simulation by (a) FLOR, (b) HiFLOR, and (d) observations from 1979 to 2012. The numbers for each basin show the annual mean number of TCs. TC tracks are colored according to the intensities of the TCs as categorized by the Saffir-Simpson hurricane wind scale [e.g., tropical depression (TD), tropical storms (TSs), and C1–C5.

FIG. 3 Model bias in TC frequency of occurrence in the 300-yr control experiments by (a) FLOR, (b) HiFLOR, and (c) restoring experiments by HiFLOR (1971–2012, mean of 6 members). The TC frequency of occurrence is defined as a total count of TC position in each analyzed 2.5° × 2.5°degree grid cell with 9-point weighting smoothing within the global domain in 6-hr intervals. The biases circled by dashed lines are above the 99% significance level estimated by a bootstrap significance test (Murakami et al. 2013).

FIG. 4 Comparisons of TC intensity. (a) Fractional ratio of annual mean TC number for the life-time maximum surface wind speed (m s^{-1}) simulated using FLOR (300 years, blue), HiFLOR (300 years, red) along with observations (1979–2012, black). (b) Maximum surface wind speed (MWS, m s^{-1}) vs minimum SLP (MSLP, hPa) for TCs using all 6-hourly data. Probability density functions [%] for MWS and MSLP are shown in histograms. The dashed black curve is the observationally based regression line proposed by Atkinson and Holiday (1977), based on observed data. Colors in (b) are same as in (a).

FIG. 5 Composite structure for TCs. (a) and (b) Mean 10-m surface wind velocity [m s^{-1}; vectors], precipitation [mm day^{-1}; shading], and sea level pressure [SLP; hPa; contours] for the control simulations by FLOR and HiFLOR, respectively. (c) Azimuthal mean tangential wind speed [m s^{-1}] for FLOR (blue) and HiFLOR (red) as a function of distance from the storm center [km]. (d)–(f) Composite daily mean SST anomaly 2 days after passages of storms (>34 kt) relative to the average over days –12 to –2 simulated by (d) FLOR, (e) HiFLOR, and (f) observations (SST: AVHRR, TC tracks: IBTrACS). The sample size (N), minimum SLP, maximum precipitation (P), and maximum tangential wind speed (TW), and minimum value in SST anomaly (MIN) in the composite are listed in each panel. Composites for (a)–(c) are for the storms at their lifetime maximum intensity in the Northern Hemisphere, whereas those for (d)–(f) are for the storms with $V/f < 1$ (i.e., slow moving or high latitude) in the all ocean basins.

FIG. 6 Composite mean SST anomaly [K] for each day before and after storm passage. SST anomaly is averaged over the domain of 100 km from the TC center relative to the average over days –12 to –2 (i.e., center of the domain for average is fixed at the storm center at day 0). Day 0 is when the storm reaches the track position, and positive (negative) days indicate the day after (before) the storm has passed. Composites are made for all storms (>34 kt) with V/f < 1 (i.e., slow moving or high latitude) in the all ocean basins.

FIG. 7 Seasonal mean variation in TC genesis number according to observations (1979–2012, grey bars) and simulation results by FLOR (300 years, blue lines) and HiFLOR (300 years, red lines) for (a) NIO, (b) WNP, (c) ENP, (d) NAT, (e) SIO, and (f) SPO. Unit is mean TC number per month.

FIG. 8 Composites of anomaly of TC frequency of occurrence for (a)–(d) El Niño years and (e)–(h) La Niña years during August–October yielded by (a), (e) observations (1979–2012), (b), (f) FLOR control simulation (300 yr), (c), (g) HiFLOR control simulation (300 yr), and (d), (h) HiFLOR restoring experiment (1971–2012, mean of 6 members). The anomalies circled by dashed lines are above the 90% significance level estimated by a bootstrap significance test (Murakami et al. 2013). Unit is 0.1 × number year^{-1}.

FIG. 9 (a) Interannual variations of annual TC genesis number in the North Atlantic according to observations and results of ensemble SST-restored experiments with HiFLOR and FLOR (1979–2012). The red (blue) line represents the mean of six ensemble experiments by

HiFLOR (FLOR). Shading indicates the range of the minimum and maximum among the six ensemble members. (b), (c) As in (a), but for TCs with hurricane intensity (>64 kt) and categories 4 and 5 intensity (>114 kt), respectively. Dashed lines denote linear trend by the Poisson regression. Only trends with statistical significance at 95% are shown [the Student t-test and modified Mann and Kendall test proposed by Hamed and Rao (1998)].

FIG. 10 Wheeler-Kiladis diagram showing zonal wavenumber-frequency power spectra of symmetric (upper panels) and antisymmetric (bottom panels) components of OLR (shadings) and phase derived from U850 (vectors) for (a) observations using AVHRR and NCEP1 (1979–2005), (b) HiFLOR (300-yr control experiment), and (c) FLOR (300-yr control experiment).

FIG. 11 Composites of TC genesis locations (red dots) superposed on anomalies of OLR (shadings) and wind at 850hPa (vectors) during boreal summer (May–October) for each MJO phase in (a) observations (1979–2005), (b) HiFLOR (300-yr control experiment), and (c) FLOR (300-yr control experiment). Composites are made when the MJO index exceeds one standard deviation. Number of days for each composite is shown in the bottom-right box.

FIG. 12 TC genesis rate for each MJO phase for each basin. For each ocean basin, the TC genesis rate is computed by dividing the number of generated TCs by the number of active-phase days of the MJO (as shown in Fig. 11). Then the fractional rate is normalized by the total rates summed over all MJO phases. Black, red, and blue lines respectively show results from observations, HiFLOR, and FLOR.

FIG. 13. Observed TC tracks during July–November for (a) 1997 and (b) 1998. (c), (d) As in (a), (b), but for retrospective prediction results for the 36-ensemble member retrospective forecast initialized on 1st July using HiFLOR. The numbers for each basin show the seasonal mean number of TCs. TC tracks are colored according to the intensities of the TCs as categorized by the Saffir-Simpson hurricane wind scale. Circles denote TC genesis locations.

FIG. 14 Difference in TC frequency of occurrence between 1997 and 1998 for all storms from (a) observations and (b) results from retrospective seasonal predictions by HiFLOR (mean of 36 members). (c), (d) As in (a), (b), but for TCs with hurricane intensity (>64 kt). (e), (f), As in (a), (b), but for TCs with categories 4 and 5 intensity (>114 kt).

FIG. 15 Box plots of the predicted number for all storms in (a) WNP, (b) ENP, and (c) NAT. (d)–(f) As in (a)–(c), but for TCs with hurricane intensity (>64 kt). (g)–(i) As in (a)–(c), but for TCs with categories 4 and 5 intensity (>114 kt). Each panel shows box plots for 1997 and 1998 using results from 36-member ensemble retrospective predictions superposed on the observed number in triangles. The boxes represent the lower and upper quartiles, the horizontal lines show the median value, and the dashed bars show the lowest datum still within the 1.5 interquartile range (IQR) of the lower quartile and the highest datum still within the 1.5 IQR of the upper quartile. Outliers are denoted in circles.

Table 1 (a) Rank correlation coefficients between the observed and simulated interannual variability of TC genesis number in the SST restored experiments for each basin. (b, c) As in (a), but for TCs with hurricane maximum winds >64 kt, and intensity categories 4 and 5 (>114 kt), respectively. 6-member SST-restored ensemble experiments are conducted using 5-day and 10-day restoring timescales each for HiFLOR and FLOR. Statistical significance is highlighted according to the level of significance: 99%, 95%, and 90% (see footnotes).

Model	NIO	WNP	ENP	NAT	SIO	SPO
			(a) All TCs			
HiFLOR	-0.30^{*}	$+0.35^{**}$	$+0.49^{***}$	$+0.68^{***}$	$+0.38^{**}$	$+0.31^{**}$
FLOR	-0.01	$+0.55^{***}$	$+0.41^{***}$	$+0.59^{***}$	$+0.02$	$+0.22$
			(b) Hurricanes (>64kt)			
HiFLOR	$+0.02$	$+0.17$	$+0.51^{***}$	$+0.77^{***}$	$+0.51^{***}$	$+0.23$
FLOR	-0.02	$+0.55^{***}$	$+0.25$	$+0.68^{***}$	$+0.10$	$+0.01$
			(c) Categories 4 and 5 (>114kt)			
HiFLOR	-0.08	$+0.23$	$+0.18$	$+0.63^{***}$	$+0.31^{**}$	$+0.12$
FLOR	*N/A*	*N/A*	*N/A*	*N/A*	*N/A*	*N/A*

*** Statistically significant at 99% level
** Statistically significant at 95% level
* Statistically significant at 90% level

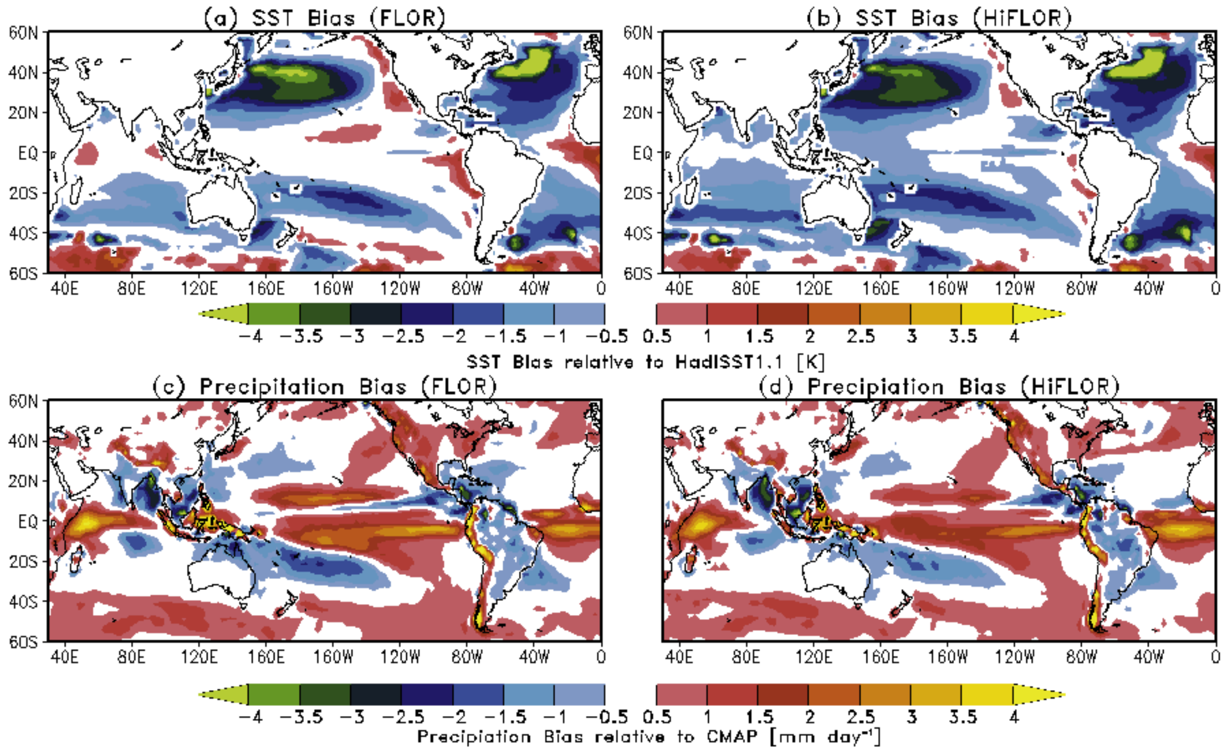

FIG. 1. Simulated biases in climatological mean SST [K] relative to HadISST1.1 during all seasons for (a) FLOR and (b) HiFLOR. (c), (d) As in (a), (b), but for precipitation [mm day^{-1}] relative to CMAP.

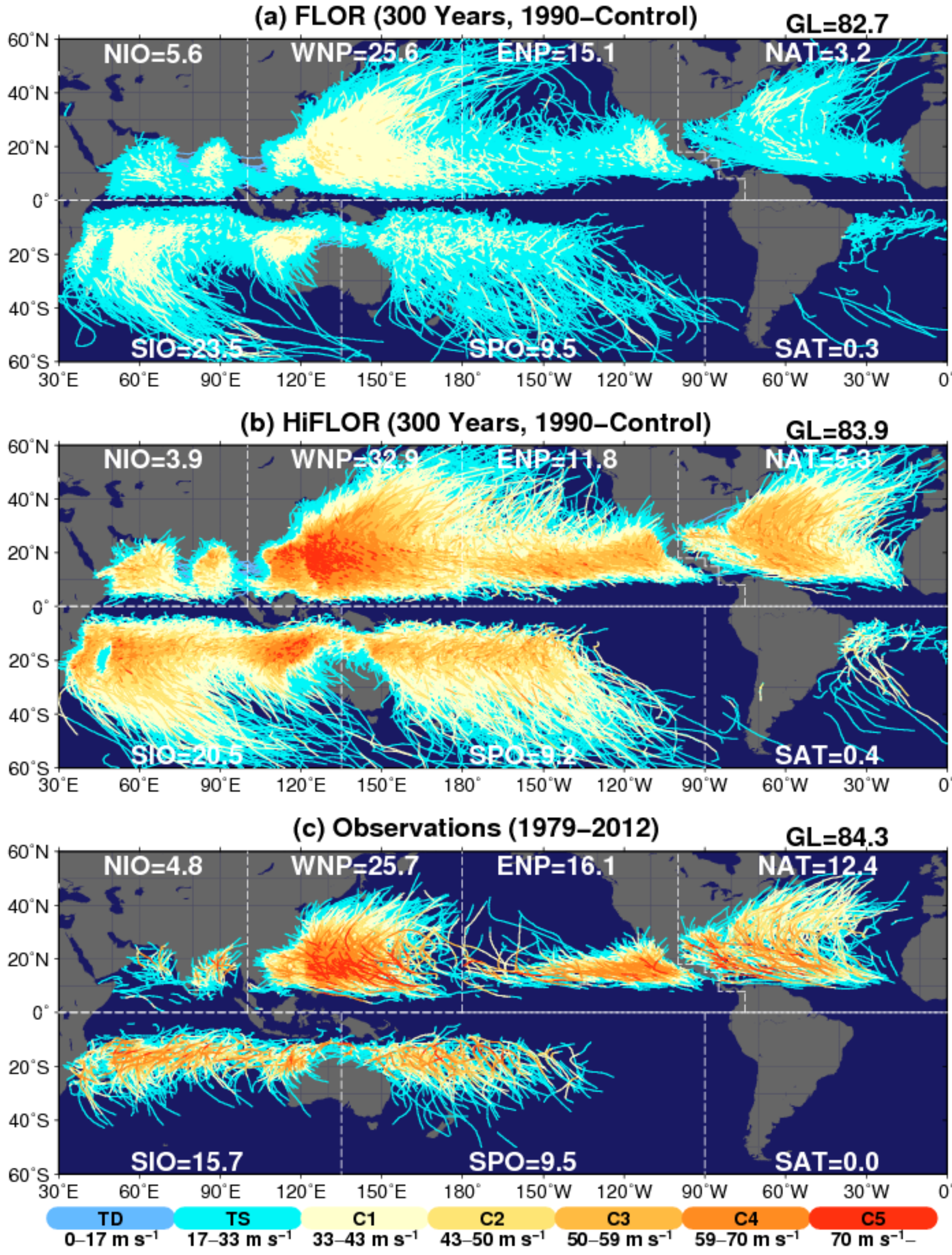

FIG. 2. Global distribution of TC tracks during all seasons for 300-year control simulation by (a) FLOR, (b) HiFLOR, and (d) observations from 1979 to 2012. The numbers for each basin show the annual mean number of TCs. TC tracks are colored according to the intensities of the TCs as categorized by the Saffir-Simpson hurricane wind scale [e.g., tropical depression (TD), tropical storms (TSs), and C1–C5.

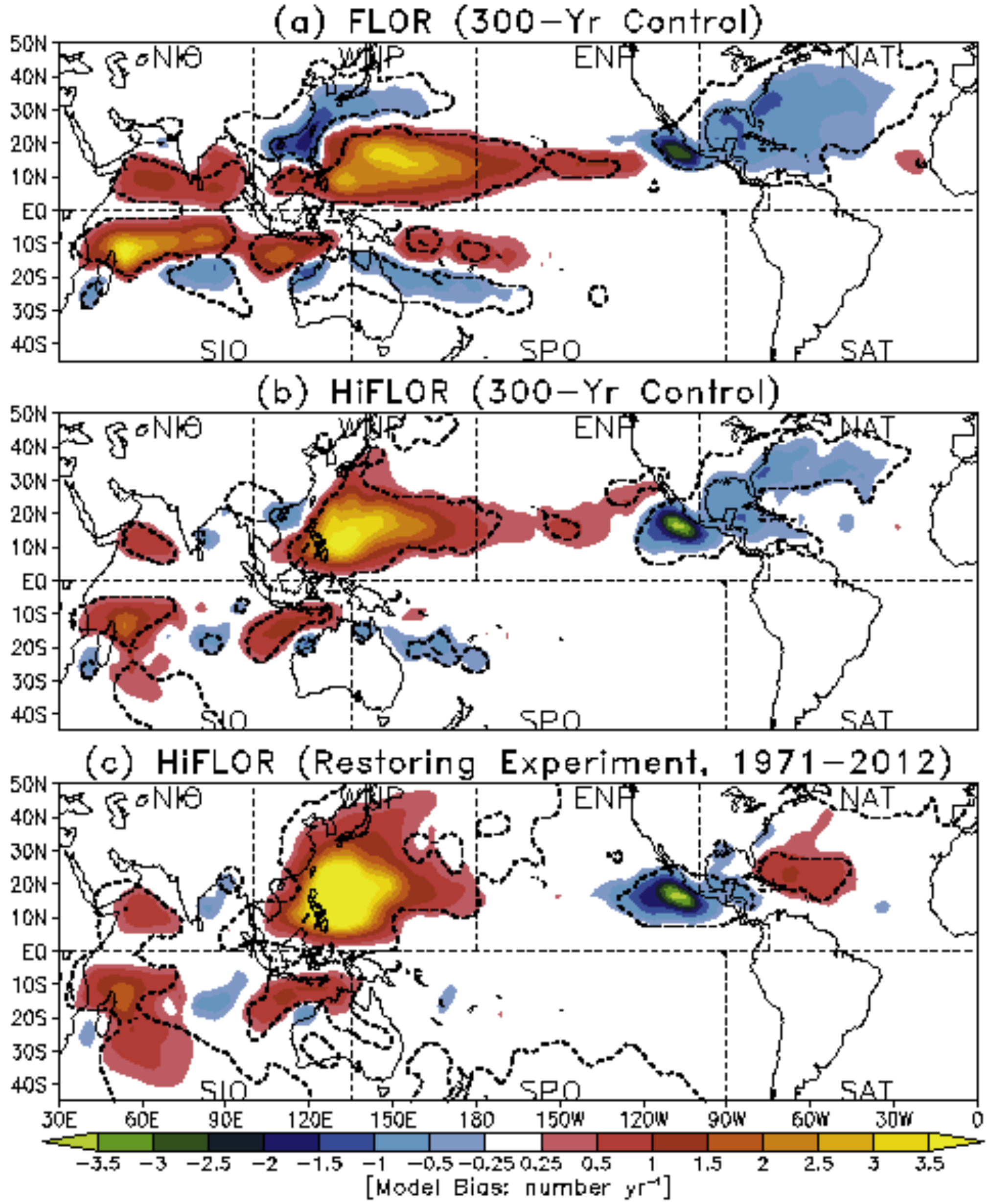

FIG. 3 Model bias in TC frequency of occurrence in the 300-yr control experiments by (a) FLOR, (b) HiFLOR, and (c) restoring experiments by HiFLOR (1971–2012, mean of 6 members). The TC frequency of occurrence is defined as a total count of TC position in each analyzed 2.5° × 2.5°degree grid cell with 9-point weighting smoothing within the global domain in 6-hr intervals. The biases circled by dashed lines are above the 99% significance level estimated by a bootstrap significance test (Murakami et al. 2013).

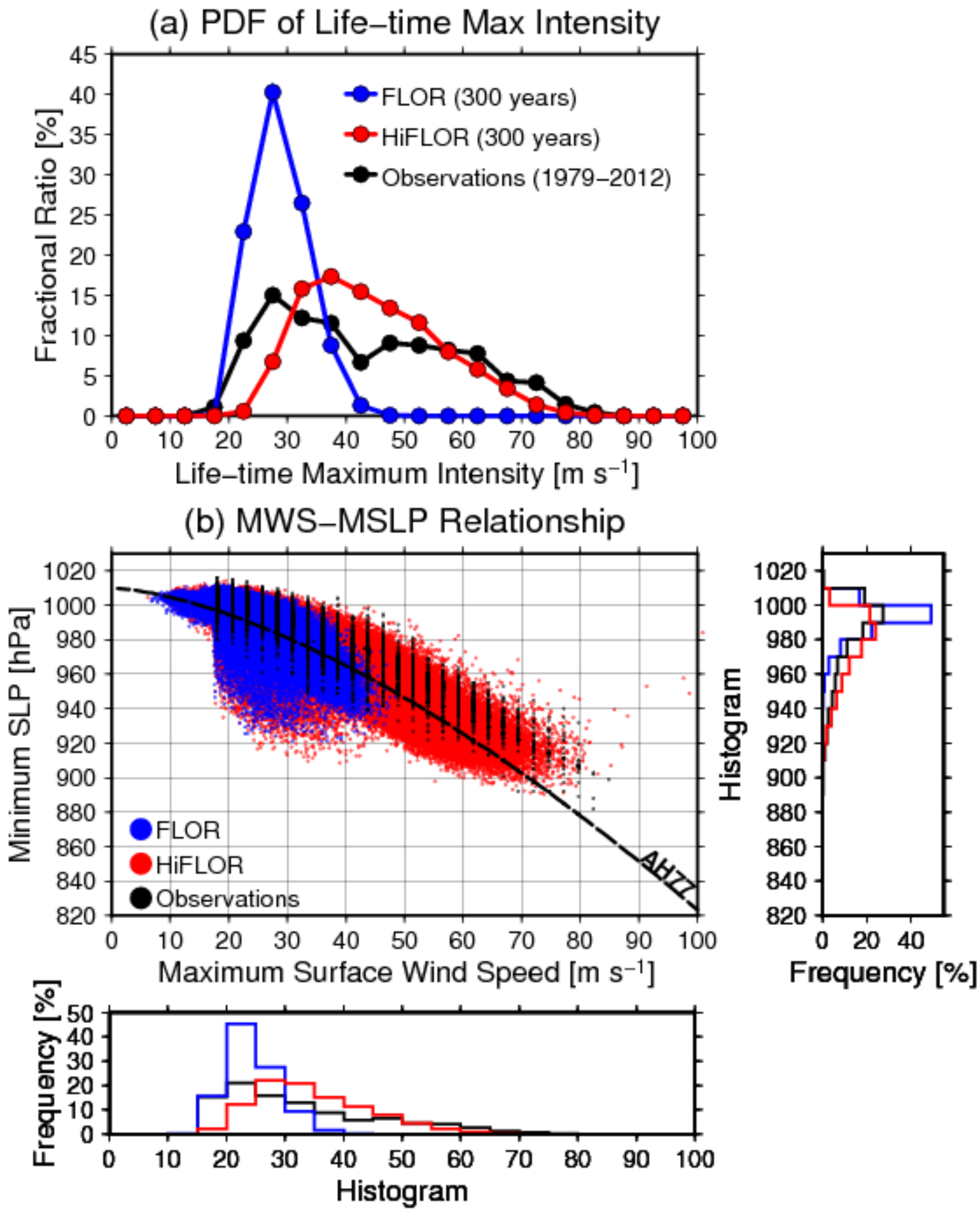

FIG. 4 Comparisons of TC intensity. (a) Fractional ratio of annual mean TC number for the life-time maximum surface wind speed (m s^{-1}) simulated using FLOR (300 years, blue), HiFLOR (300 years, red) along with observations (1979–2012, black). (b) Maximum surface wind speed (MWS, m s^{-1}) vs minimum SLP (MSLP, hPa) for TCs using all 6-hourly data. Probability density functions [%] for MWS and MSLP are shown in histograms. The dashed black curve is the observationally based regression line proposed by Atkinson and Holiday (1977), based on observed data. Colors in (b) are same as in (a).

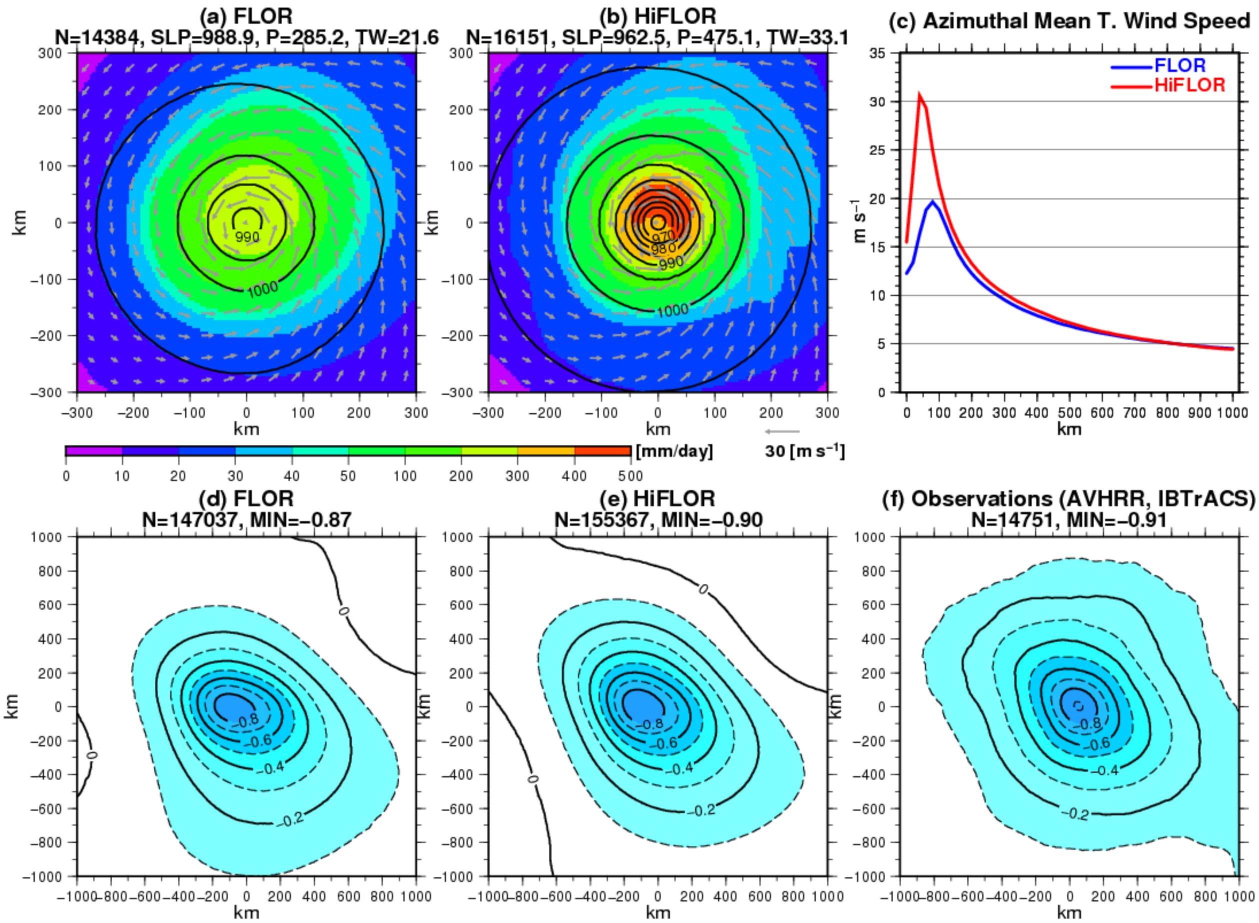

FIG. 5 Composite structure for TCs. (a) and (b) Mean 10-m surface wind velocity [m s^{-1}; vectors], precipitation [mm day^{-1}; shading], and sea level pressure [SLP; hPa; contours] for the control simulations by FLOR and HiFLOR, respectively. (c) Azimuthal mean tangential wind speed [m s^{-1}] for FLOR (blue) and HiFLOR (red) as a function of distance from the storm center [km]. (d)–(f) Composite daily mean SST anomaly 2 days after passages of storms (>34 kt) relative to the average over days –12 to –2 simulated by (d) FLOR, (e) HiFLOR, and (f) observations (SST: AVHRR, TC tracks: IBTrACS). The sample size (N), minimum SLP, maximum precipitation (P), and maximum tangential wind speed (TW), and minimum value in SST anomaly (MIN) in the composite are listed in each panel. Composites for (a)–(c) are for the storms at their lifetime maximum intensity in the Northern Hemisphere, whereas those for (d)–(f) are for the storms with V/f < 1 (i.e., slow moving or high latitude) in the all ocean basins.

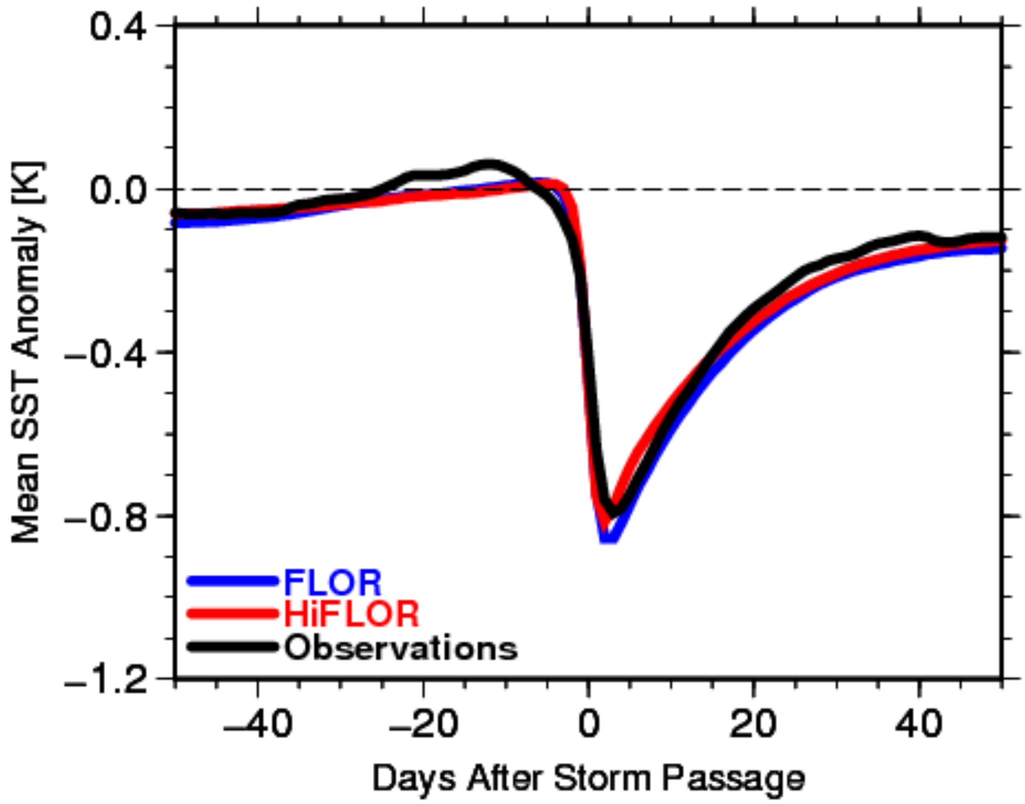

FIG. 6 Composite mean SST anomaly [K] for each day before and after storm passage. SST anomaly is averaged over the domain of 100 km from the TC center relative to the average over days –12 to –2 (i.e., center of the domain for average is fixed at the storm center at day 0). Day 0 is when the storm reaches the track position, and positive (negative) days indicate the day after (before) the storm has passed. Composites are made for all storms (>34 kt) with V/f < 1 (i.e., slow moving or high latitude) in the all ocean basins.

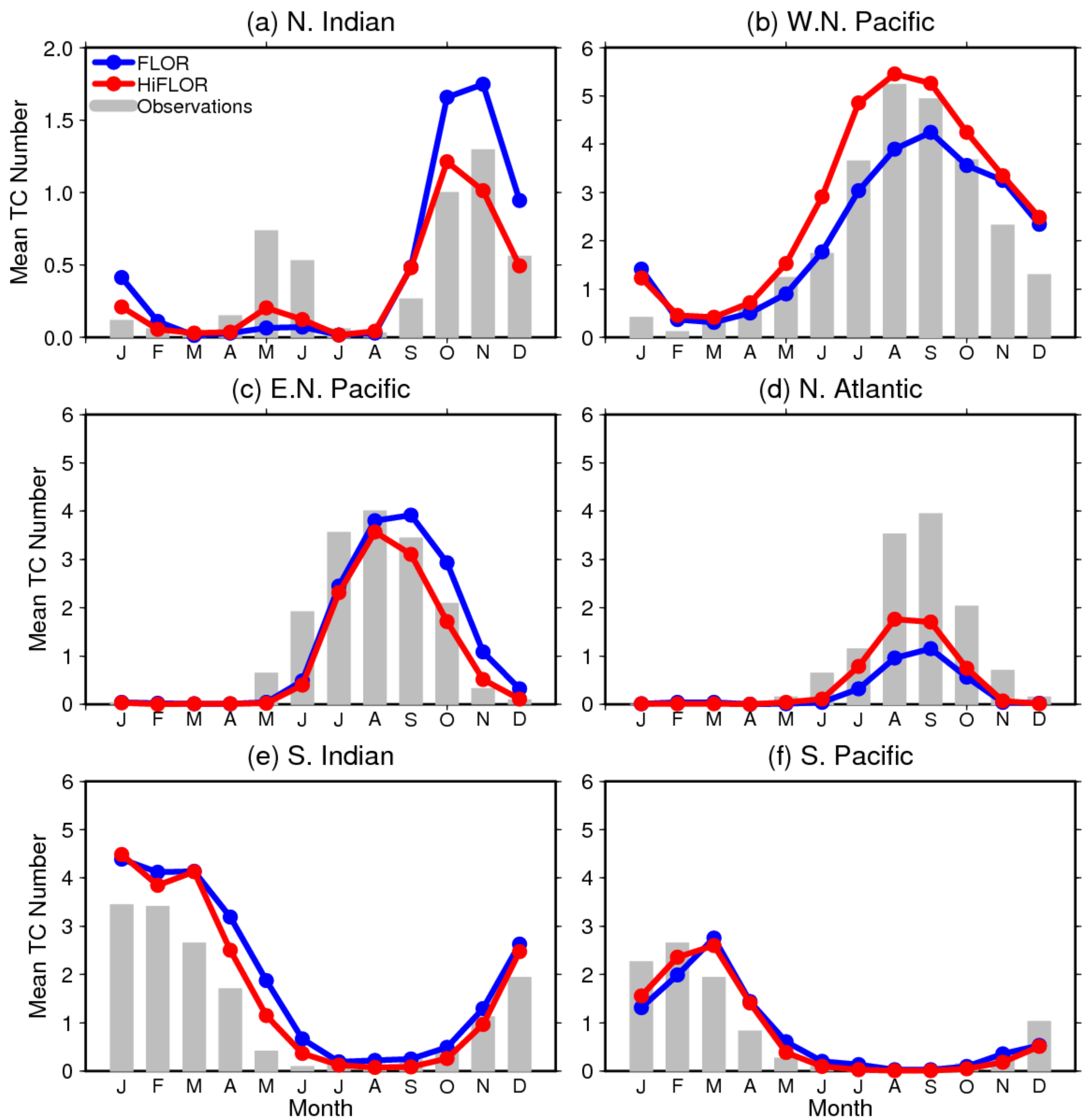

FIG. 7 Seasonal mean variation in TC genesis number according to observations (1979–2012, grey bars) and simulation results by FLOR (300 years, blue lines) and HiFLOR (300 years, red lines) for (a) NIO, (b) WNP, (c) ENP, (d) NAT, (e) SIO, and (f) SPO. Unit is mean TC number per month.

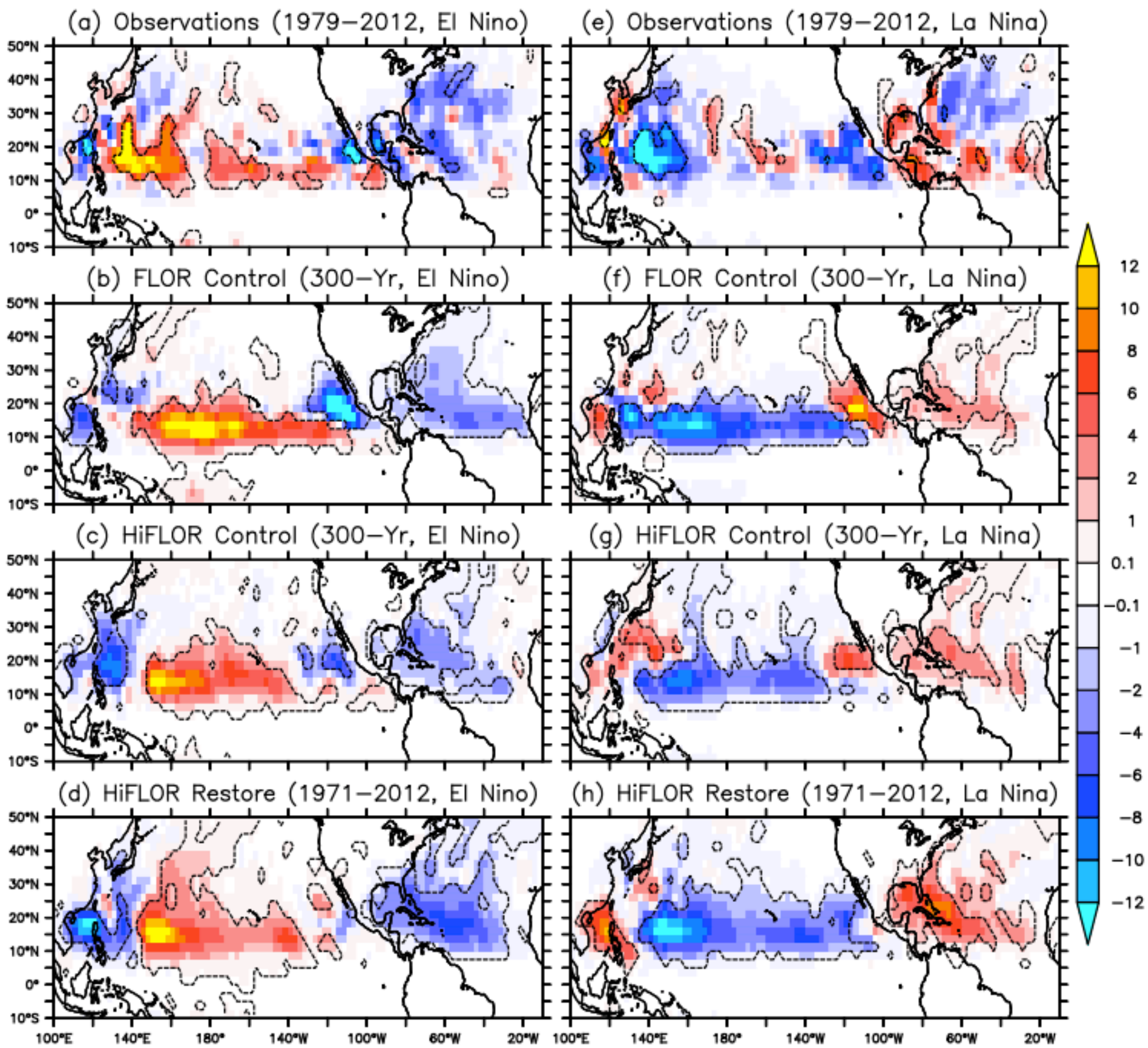

FIG. 8 Composites of anomaly of TC frequency of occurrence for (a)–(d) El Niño years and (e)–(h) La Niña years during August–October yielded by (a), (e) observations (1979–2012), (b), (f) FLOR control simulation (300 yr), (c), (g) HiFLOR control simulation (300 yr), and (d), (h) HiFLOR restoring experiment (1971–2012, mean of 6 members). The anomalies circled by dashed lines are above the 90% significance level estimated by a bootstrap significance test (Murakami et al. 2013). Unit is 0.1 × number year^{-1}.

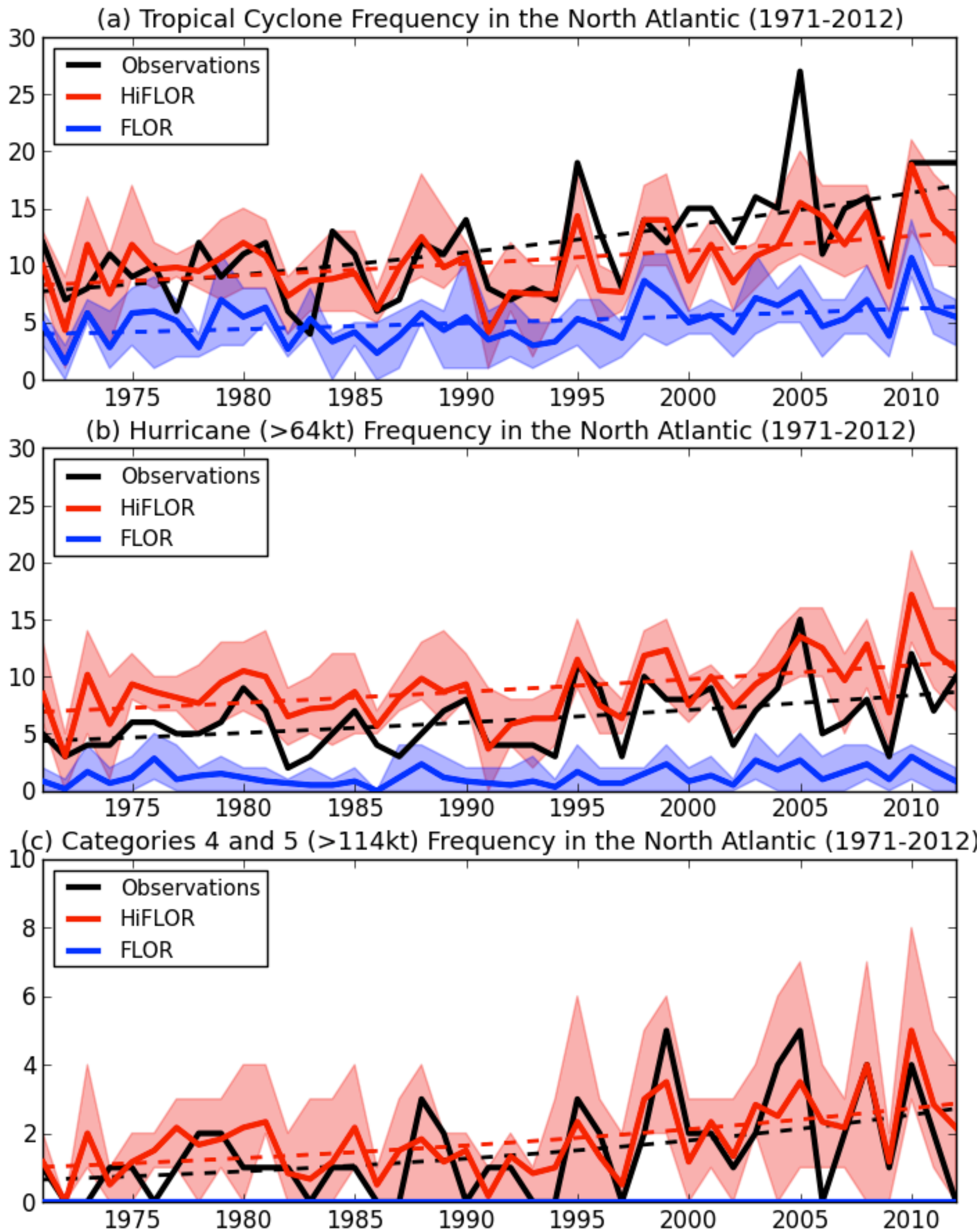

FIG. 9 (a) Interannual variations of annual TC genesis number in the North Atlantic according to observations and results of ensemble SST-restored experiments with HiFLOR and FLOR (1979–2012). The red (blue) line represents the mean of six ensemble experiments by HiFLOR (FLOR). Shading indicates the range of the minimum and maximum among the six ensemble members. (b), (c) As in (a), but for TCs with hurricane intensity (>64 kt) and categories 4 and 5 intensity (>114 kt), respectively. Dashed lines denote linear trend by the Poisson regression. Only trends with statistical significance at 95% are shown [the Student t-test and modified Mann and Kendall test proposed by Hamed and Rao (1998)].

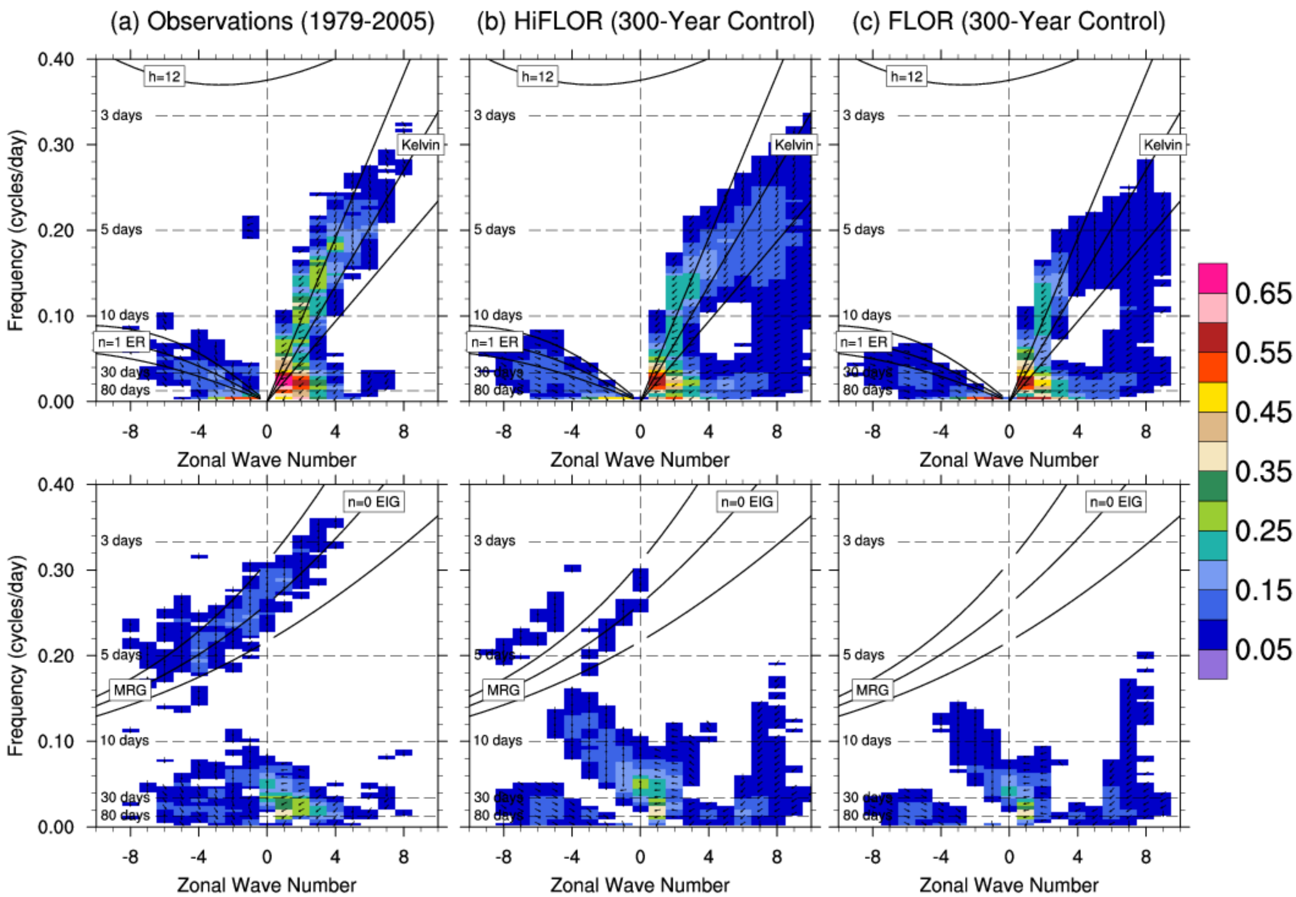

FIG. 10 Wheeler-Kiladis diagram showing zonal wavenumber-frequency power spectra of symmetric (upper panels) and antisymmetric (bottom panels) components of OLR (shadings) and phase derived from U850 (vectors) for (a) observations using AVHRR and NCEP1 (1979–2005), (b) HiFLOR (300-yr control experiment), and (c) FLOR (300-yr control experiment).

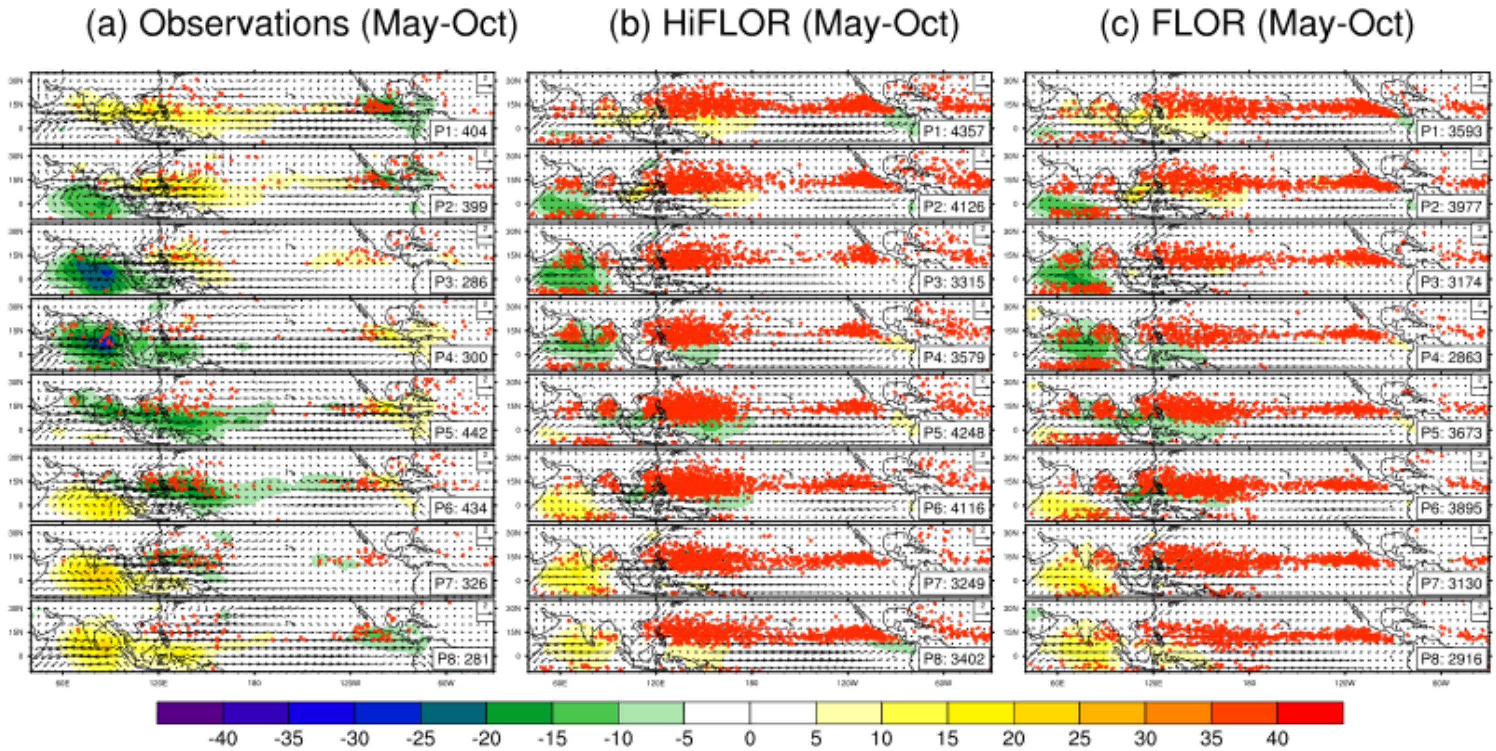

FIG. 11 Composites of TC genesis locations (red dots) superposed on anomalies of OLR (shadings) and wind at 850hPa (vectors) during boreal summer (May–October) for each MJO phase in (a) observations (1979–2005), (b) HiFLOR (300-yr control experiment), and (c) FLOR (300-yr control experiment). Composites are made when the MJO index exceeds one standard deviation. Number of days for each composite is shown in the bottom-right box.

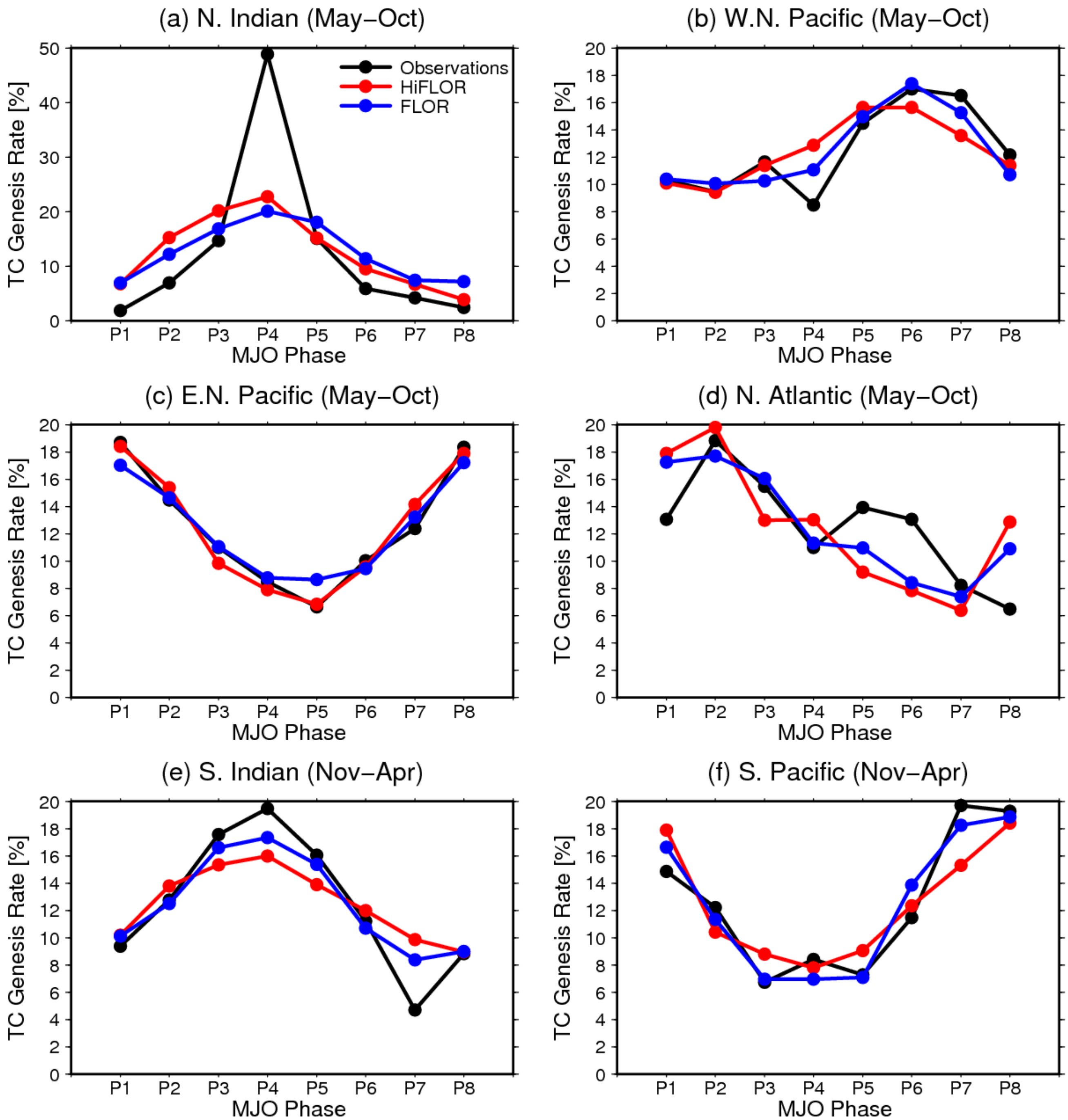

FIG. 12 TC genesis rate for each MJO phase for each basin. For each ocean basin, the TC genesis rate is computed by dividing the number of generated TCs by the number of active-phase days of the MJO (as shown in Fig. 11). Then the fractional rate is normalized by the total rates summed over all MJO phases. Black, red, and blue lines respectively show results from observations, HiFLOR, and FLOR.

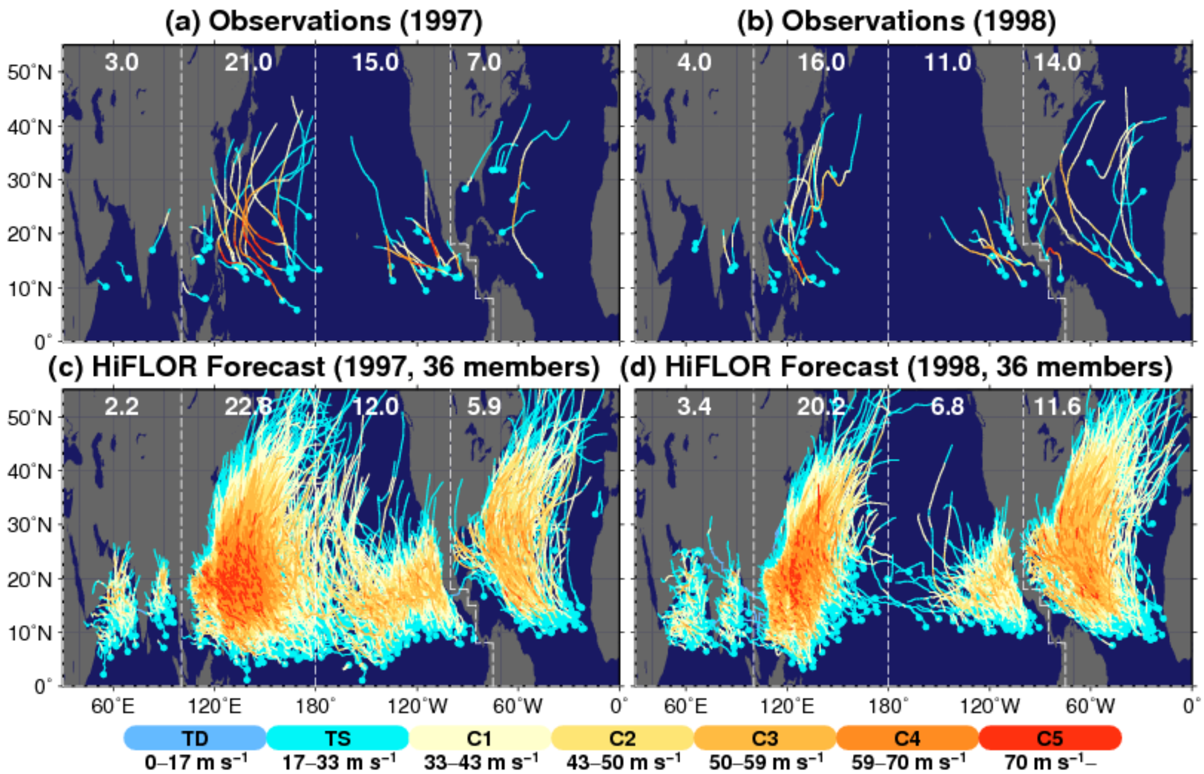

FIG. 13. Observed TC tracks during July–November for (a) 1997 and (b) 1998. (c), (d) As in (a), (b), but for retrospective prediction results for the 36-ensemble member retrospective forecast initialized on 1st July using HiFLOR. The numbers for each basin show the seasonal mean number of TCs. TC tracks are colored according to the intensities of the TCs as categorized by the Saffir-Simpson hurricane wind scale. Circles denote TC genesis locations.

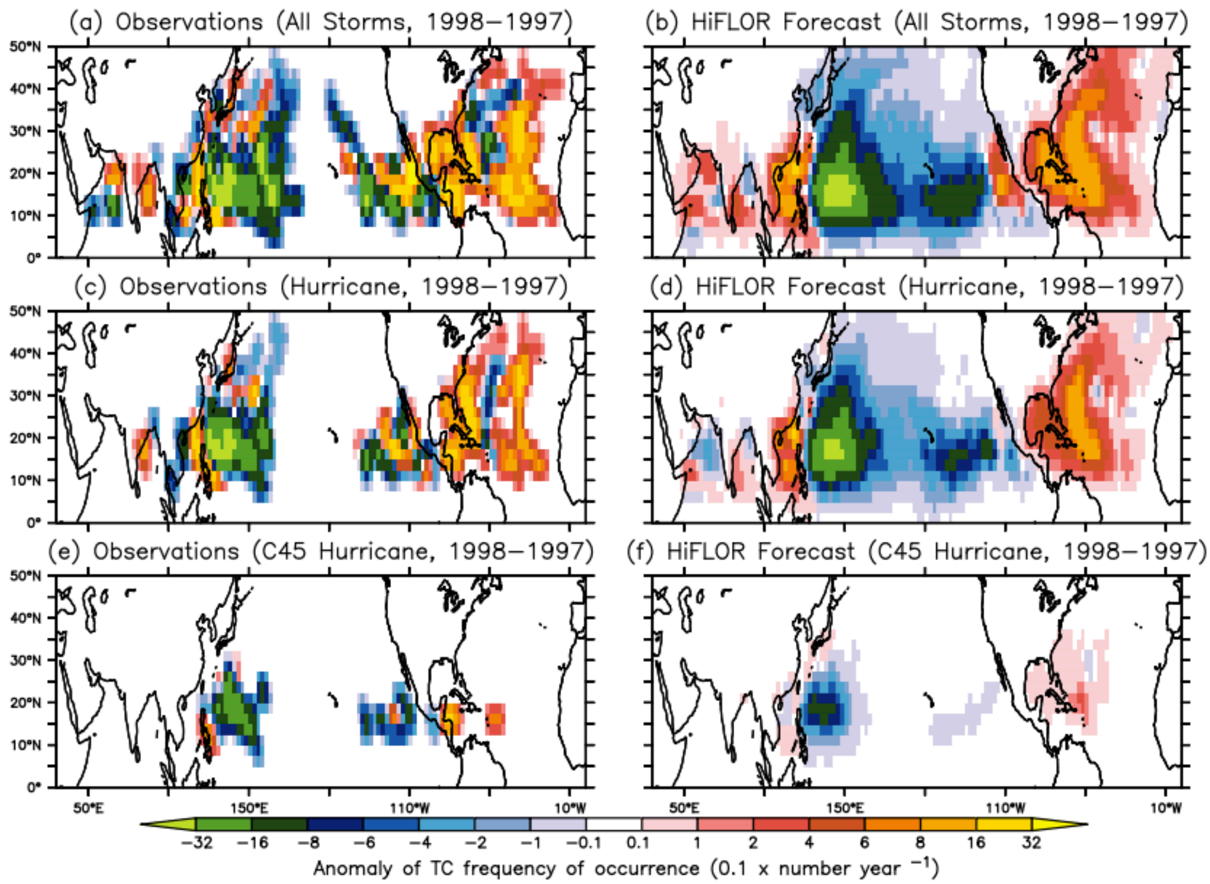

FIG. 14 Difference in TC frequency of occurrence between 1997 and 1998 for all storms from (a) observations and (b) results from retrospective seasonal predictions by HiFLOR (mean of 36 members). (c), (d) As in (a), (b), but for TCs with hurricane intensity (>64 kt). (e), (f), As in (a), (b), but for TCs with categories 4 and 5 intensity (>114 kt).

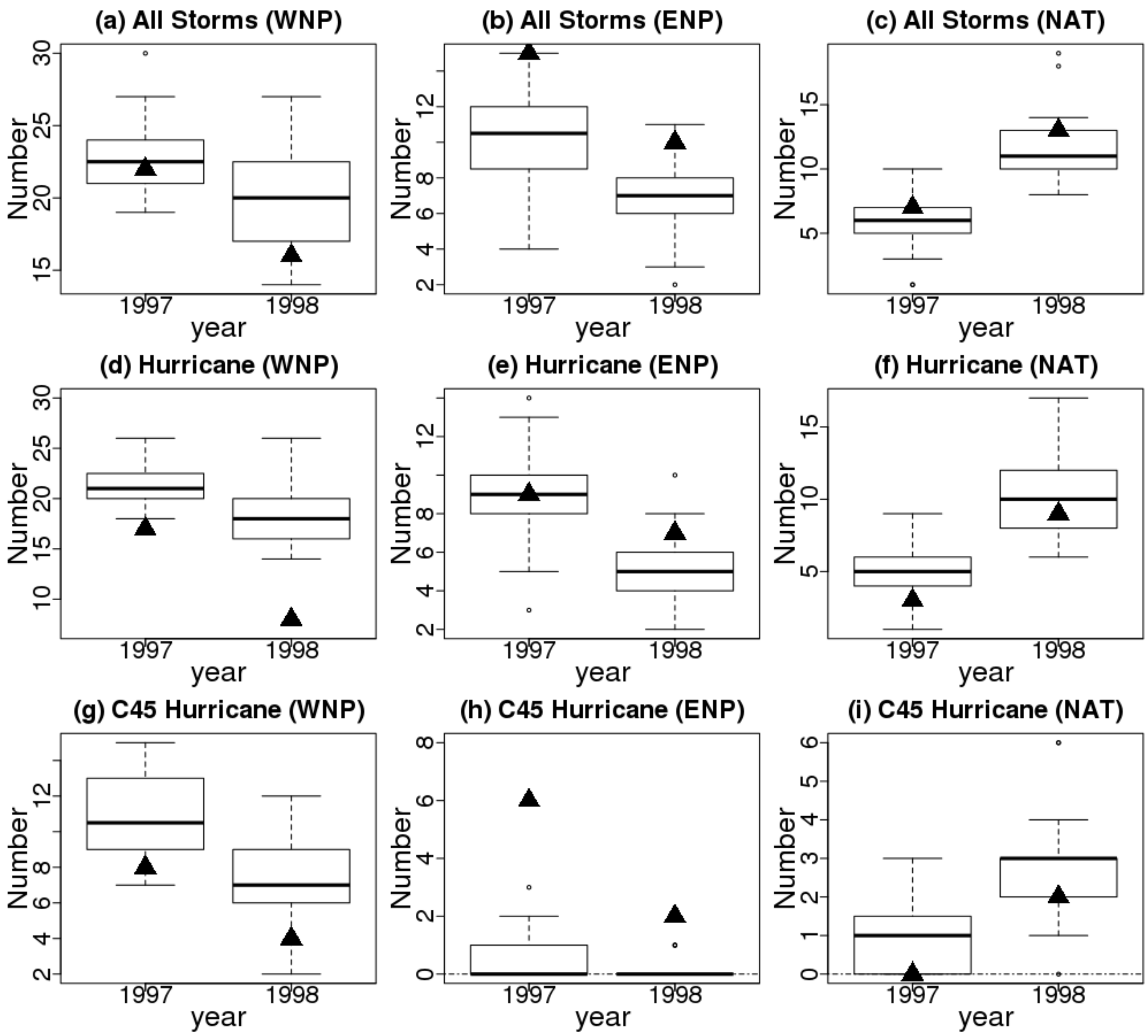

FIG. 15 Box plots of the predicted number for all storms in (a) WNP, (b) ENP, and (c) NAT. (d)–(f) As in (a)–(c), but for TCs with hurricane intensity (>64 kt). (g)–(i) As in (a)–(c), but for TCs with categories 4 and 5 intensity (>114 kt). Each panel shows box plots for 1997 and 1998 using results from 36-member ensemble retrospective predictions superposed on the observed number in triangles. The boxes represent the lower and upper quartiles, the horizontal lines show the median value, and the dashed bars show the lowest datum still within the 1.5 interquartile range (IQR) of the lower quartile and the highest datum still within the 1.5 IQR of the upper quartile. Outliers are denoted in circles.